

1       **ACCURACY OF SPECTRAL ELEMENT METHOD FOR WAVE,**  
2       **PARABOLIC AND SCHRÖDINGER EQUATIONS \***

3               HAO LI<sup>†</sup>, DANIEL APPELÖ<sup>‡</sup>, AND XIANGXIONG ZHANG<sup>†</sup>

4       **Abstract.** The spectral element method constructed by the  $Q^k$  ( $k \geq 2$ ) continuous finite  
5 element method with  $(k + 1)$ -point Gauss-Lobatto quadrature on rectangular meshes is a popular  
6 high order scheme for solving wave equations in various applications. It can also be regarded as a  
7 finite difference scheme on all Gauss-Lobatto points. We prove that this finite difference scheme is  
8  $(k + 2)$ -order accurate in discrete 2-norm for smooth solutions. The same proof can be extended to  
9 the spectral element method solving linear parabolic and Schrödinger equations. The main result  
10 also applies to the spectral element method on curvilinear meshes that can be smoothly mapped to  
11 rectangular meshes on the unit square.

12       **Key words.** Spectral element method, Gauss-Lobatto quadrature, superconvergence, the wave  
13 equation, parabolic equations, the linear Schrödinger equation.

14       **AMS subject classifications.** 65M60, 65M15, 65M06

15       **1. Introduction.** Accurate and efficient approximations of solutions to partial  
16 differential equations are important to numerous applications arising in engineering  
17 and the sciences. In particular for problems whose solutions are of wave type, high  
18 order accurate methods are favored as they can control the dispersive errors in wave  
19 forms that propagate over vast distances.

20       For wave equations and other hyperbolic problems, the two key insights that  
21 a numerical analyst can provide to a practitioner comparing methods are: a) if the  
22 method is guaranteed to be stable, and b) if the numerical method is guaranteed to be  
23 accurate. The first condition is most conveniently guaranteed by selecting a method  
24 that is based on a variational formulation such as spectral elements, summation-by-  
25 parts s and continuous and discontinuous Galerkin finite element methods.

26       In recent years many such stable and high order accurate methods for wave equa-  
27 tions have been developed. These include discontinuous Galerkin methods for first  
28 order hyperbolic systems [17, 31, 7, 8, 18, 40, 30] and wave equations in second or-  
29 der form [32, 15, 6, 2], and finite differences with summation by parts operators  
30 [27, 29, 28, 36, 1, 38, 39], as well as spectral elements for wave equations [21, 20].

31       In this paper we are mainly concerned with the second topic, to provide rigorous  
32 estimates on the errors for a method. In particular, we study the rates of convergence  
33 of the error, as measured in norms over nodes for all degree of freedoms, for the spectral  
34 element method applied to linear wave and parabolic, and Schrödinger equations.  
35 These three types of equations are fundamentally different, but all of them contain  
36 the same second order operator, which can be discretized by the same spectral element  
37 method.

38       To be precise, we consider the Lagrangian  $Q^k$  ( $k \geq 2$ ) continuous finite element  
39 method for solving linear evolution PDEs with a second order operator  $\nabla \cdot (\mathbf{a}(\mathbf{x})\nabla u)$   
40 on rectangular meshes implemented by  $(k + 1)$ -point Gauss-Lobatto quadrature for

---

\*H. Li and X. Zhang were supported by the NSF grant DMS-1522593. D. Appelö was supported in part by NSF Grant DMS-1913076. Any conclusions or recommendations expressed in this paper are those of the authors and do not necessarily reflect the views of the NSF.

<sup>†</sup>Department of Mathematics, Purdue University, 150 N. University Street, West Lafayette, IN 47907-2067 (li2497@purdue.edu, zhan1966@purdue.edu).

<sup>‡</sup>Department of Computational Mathematics, Science, and Engineering; Department of Mathematics, Michigan State University, East Lansing, MI 48824 (appeloda@msu.edu).

all integrals. This is often referred to as the spectral element method in the literature and this is the notation we will use here.

For the  $Q^k$  spectral element method, it is well known that the standard finite element error estimates still hold [26], i.e., the error in  $H^1$ -norm is  $k$ -th order and the error in  $L^2$ -norm is  $(k+1)$ -th order. It is also well known that the Lagrangian  $Q^k$  ( $k \geq 2$ ) continuous finite element method is  $(k+2)$ -th order accurate in the discrete 2-norm over all  $(k+1)$ -point Gauss-Lobatto quadrature points [37, 25, 3]. If using a very accurate quadrature in the finite element method for a variable coefficient operator  $\nabla \cdot (\mathbf{a}(\mathbf{x})\nabla u)$ , then  $(k+2)$ -th order superconvergence at Gauss-Lobatto points holds trivially. However, for the efficiency of having a diagonal mass matrix and for the convenience of implementation, the most popular method for wave equations is the simplest choice of quadrature, i.e. using  $(k+1)$ -point Gauss-Lobatto quadrature for  $Q^k$  elements in all integrals for both mass and stiffness matrices. In particular in the seismic community, where highly efficient simulation of the elastic wave equation is of important, the spectral method has become the method of choice, [21, 20].

When using this  $(k+1)$ -point Gauss-Lobatto quadrature for Lagrangian  $Q^k$  finite element method, the quadrature nodes coincide with the nodes defining the degrees of freedom, and the resulting method becomes the so-called spectral element method. Thus the spectral element method can also be regarded as a finite difference scheme at all Gauss-Lobatto points. For instance, consider solving  $u_{tt} = u_{xx}$  on the interval  $[0, 1]$  with homogeneous Dirichlet boundary conditions. Introduce the uniform grid  $0 = x_0 < x_1 < \dots < x_N < x_{N+1} = 1$  with spacing  $h = 1/(N+1)$  and  $N$  being odd. This grid gives a uniform partition of the interval  $[0, 1]$  into uniform intervals  $I_k = [x_{2k}, x_{2k+2}]$  ( $k = 0, \dots, \frac{N-1}{2}$ ). Then all 3-point Gauss-Lobatto quadrature points for intervals  $I_k = [x_{2k}, x_{2k+2}]$  coincide with the grid points  $x_i$ . The  $Q^2$  spectral element method on intervals  $I_k = [x_{2k}, x_{2k+2}]$  ( $k = 0, \dots, \frac{N-1}{2}$ ) is equivalent to the following semi-discrete finite difference scheme [9, 24]:

$$(1.1a) \quad \frac{d^2}{dt^2} u_i = \frac{u_{i-1} - 2u_i + u_{i+1}}{h^2}, \quad \text{if } i \text{ is odd};$$

$$(1.1b) \quad \frac{d^2}{dt^2} u_i = \frac{-u_{i-2} + 8u_{i-1} - 14u_i + 8u_{i+1} - u_{i+2}}{4h^2}, \quad \text{if } i \text{ is even}.$$

While the truncation error of (1.1) is only second order yet the dispersion error is fourth order, see Section 11 in [9]. Although the dispersion error results can in principle be extended to any order, the derivation and expressions become increasingly cumbersome. Further the dispersion error results are limited to unbounded or periodic domains and do not produce error estimates in the form of a norm of the error. Other than spectral element methods, other high order schemes can also be interpreted as a finite difference scheme, such as the Fourier pseudo-spectral method [5, 13, 4].

In fact, as we have shown in [24], it is nontrivial and requires new analysis tools to establish the  $(k+2)$ -th order superconvergence when  $(k+1)$ -point Gauss-Lobatto quadrature is used. In [24],  $(k+2)$ -th order accuracy at all Gauss-Lobatto points of  $Q^k$  spectral element method was proven for elliptic equations with Dirichlet boundary conditions. In this paper, we extend those results and will prove that the  $Q^k$  spectral element method is a  $(k+2)$ -th order accurate scheme for linear wave, parabolic and Schrödinger equations with Dirichlet boundary conditions. For Neumann boundary conditions, if  $\mathbf{a}(\mathbf{x})$  is diagonal, i.e., there are no mixed second order derivatives in  $\nabla \cdot (\mathbf{a}(\mathbf{x})\nabla u)$ ,  $(k+2)$ -th order accuracy in discrete 2-norm can be proven. When mixed second order derivatives are involved, only  $(k + \frac{3}{2})$ -th order can be proven for

88 Neumann boundary conditions, and we indeed observe some order loss in numerical  
89 tests.

90 The main contribution of this paper is to explain the order of accuracy of  $Q^k$   
91 spectral element method, when the errors are measured only at nodes of degree of  
92 freedoms. As mentioned above we consider the case of rectangular elements and  
93 a smooth coefficient  $\mathbf{a}(\mathbf{x})$  in the term  $\nabla \cdot (\mathbf{a}(\mathbf{x})\nabla u)$ . We note that this does include  
94 discretizations on regular meshes of curvilinear domains that can be smoothly mapped  
95 to rectangular meshes for the unit cube, e.g., the spectral element method for  $\Delta u$  on  
96 such a mesh for a curvilinear domain is equivalent to the spectral element method for  
97  $\nabla \cdot (\mathbf{a}(\mathbf{x})\nabla u) + \mathbf{b}(\mathbf{x}) \cdot \nabla u$  on a reference uniform rectangular mesh where  $\mathbf{a}(\mathbf{x})$  and  $\mathbf{b}(\mathbf{x})$   
98 emerge from the mapping between the curvilinear domain and the unit cube. It does  
99 however not include problems on unstructured quadrilateral meshes where the metric  
100 terms typically are non-smooth at element interfaces but we note that the numerical  
101 examples that we present indicate that such meshes may still exhibit larger rates than  
102  $k + 1$ . We only consider the semi-discrete schemes for linear equations in this paper.  
103 In general, it is straightforward to extend the error estimates to a fully discrete scheme  
104 for simple time discretizations, e.g., [41]. Even though superconvergence in  $Q^k$  finite  
105 element method without any quadrature can be established for nonlinear equations  
106 [3], the result in this paper may no longer hold for generic nonlinear equations since  
107 the simplest  $(k + 1)$ -point Gauss-Lobatto quadrature are not accurate enough for  
108 nonlinear terms.

109 This paper is organized as follows. In Section 2, we introduce notation and  
110 assumptions. In Section 3, we review a few standard quadrature estimates. In Section  
111 4, the superconvergence of elliptic projection is analyzed, which is parallel to the classic  
112 error estimation for hyperbolic and parabolic equations by involving elliptic projection  
113 of the corresponding elliptic operator, see [41, 33, 11]. We then prove the main  
114 result for homogeneous Dirichlet boundary conditions in Section 5, for the second-  
115 order wave equation in Section 5.1, parabolic equations in Section 5.2 and linear  
116 Schrödinger equation in Section 5.3. Neumann boundary conditions can be discussed  
117 similarly as summarized in Section 5.4. For problems with nonhomogeneous Dirichlet  
118 boundary conditions, a convenient implementation which maintains the  $(k + 2)$ -th  
119 order of accuracy is given in Section 6. Numerical tests verifying the estimates are  
120 given in Section 7. Concluding remarks are given in Section 8

## 121 2. Equations, notation, and assumptions.

122 **2.1. Problem setup.** Let  $L$  be a linear second order differential operator with  
123 time dependent coefficients:

$$124 \quad Lu = -\nabla \cdot (\mathbf{a}(\mathbf{x}, t)\nabla u) + \mathbf{b}(\mathbf{x}, t) \cdot \nabla u + c(\mathbf{x}, t)u,$$

126 where  $\mathbf{a}(\mathbf{x}, t) = (a_{ij}(\mathbf{x}, t))$  is a positive symmetric definite operator for  $t \in [0, T]$ ,  
127 i.e. there exist constants  $\alpha, \beta > 0$  such that  $\alpha|\xi|^2 \leq \xi^T \mathbf{a}(\mathbf{x}, t)\xi \leq \beta|\xi|^2$ , for all  
128  $(\mathbf{x}, t) \in \Omega \times [0, T], \xi \in \mathbb{R}^n$ . Consider the following two initial-boundary value problems  
129 with smooth enough coefficients on a rectangular domain  $\Omega = (0, 1) \times (0, 1)$  with its  
130 boundary  $\partial\Omega$ :

131 Given  $0 < T < \infty$ , find  $u(\mathbf{x}, t)$  on  $\bar{\Omega} \times [0, T]$  satisfying

$$132 \quad (2.1) \quad \begin{aligned} u_t &= -Lu + f(\mathbf{x}, t) && \text{in } \Omega \times (0, T], \\ u(\mathbf{x}, t) &= 0 && \text{on } \partial\Omega \times [0, T], \\ u(\mathbf{x}, 0) &= u_0(\mathbf{x}) && \text{on } \Omega. \end{aligned}$$

133 Given  $0 < T < \infty$ , find  $u(\mathbf{x}, t)$  on  $\bar{\Omega} \times [0, T]$  satisfying

$$134 \quad (2.2) \quad \begin{aligned} u_{tt} &= -Lu + f(\mathbf{x}, t) && \text{in } \Omega \times (0, T], \\ u(\mathbf{x}, t) &= 0 && \text{on } \partial\Omega \times [0, T], \\ u(\mathbf{x}, 0) &= u_0(\mathbf{x}), \quad u_t(\mathbf{x}, 0) = u_1(\mathbf{x}) && \text{on } \Omega \times \{t = 0\}. \end{aligned}$$

135 We use  $A(\cdot)$  to denote the bilinear form: for  $u, v \in H^1(\Omega)$ ,

$$136 \quad (2.3) \quad A(u, v) = \int_{\Omega} \nabla u^T \mathbf{a}(\mathbf{x}, t) \nabla v + \mathbf{b}(\mathbf{x}, t) \cdot \nabla u + c(\mathbf{x}, t) uv \, d\mathbf{x}.$$

138 For convenience, we assume  $\Omega_h$  is a uniform rectangular mesh for  $\bar{\Omega}$  and  $e = [x_e -$   
 139  $h, x_e + h] \times [y_e - h, y_e + h]$  denotes any cell in  $\Omega_h$  with cell center  $(x_e, y_e)$ . Though we only  
 140 discuss uniform meshes, the main result can be easily extended to nonuniform rectan-  
 141 gular meshes with smoothly varying cells. Let  $Q^k(e) = \left\{ p(x, y) = \sum_{i=0}^k \sum_{j=0}^k p_{ij} x^i y^j, (x, y) \in e \right\}$ ,  
 142 denote the set of tensor product of polynomials of degree  $k$  on an element  $e$ . Then  
 143 we use  $V^h = \{p(x, y) \in C^0(\Omega_h) : p|_e \in Q^k(e), \forall e \in \Omega_h\}$  to denote the continu-  
 144 ous piecewise  $Q^k$  finite element space on  $\Omega_h$  and  $V_0^h = \{v_h \in V^h : v_h|_{\partial\Omega} = 0\}$ . Let  
 145  $(u, v) = \int_{\Omega} uv \, d\mathbf{x}$  and let  $\langle \cdot, \cdot \rangle_h$  and  $A_h(\cdot, \cdot)$  denote approximation of the integrals by  
 146  $(k+1)$ -point Gauss-Lobatto quadrature for each spatial variable in each cell. Also,  
 147  $u^{(i)}$  will denote the  $i$ -th time derivative of the function  $u(\mathbf{x}, t)$ .

148 For the equations that we are interested in, assume the exact solution  $u(\mathbf{x}, t) \in$   
 149  $H_0^1(\Omega) \cap H^2(\Omega)$  for any  $t$ , and define its discrete elliptic projection  $R_h u \in V_0^h$  as

$$150 \quad (2.4) \quad A_h(R_h u, v_h) = \langle -Lu, v_h \rangle_h, \quad \forall v_h \in V_0^h, \quad 0 \leq t \leq T.$$

151 Also, let  $u_I \in V^h$  denote the piecewise Lagrangian  $Q^k$  interpolation polynomial of  
 152 function  $u$  at  $(k+1) \times (k+1)$  Gauss-Lobatto points in each rectangular cell.

153 We consider semi-discrete spectral element schemes whose initial conditions are  
 154 defined by the elliptic projection and the Lagrange interpolant of the continuous initial  
 155 data.

156 For problem (2.1) the scheme is to find  $u_h(\mathbf{x}, t) \in V_0^h$  satisfying

$$157 \quad (2.5) \quad \begin{aligned} \langle u_h^{(1)}, v_h \rangle_h + A_h(u_h, v_h) &= \langle f, v_h \rangle_h, \quad \forall v_h \in V_0^h, \\ u_h(0) &= R_h u_0. \end{aligned}$$

158 We consider the semi-discrete spectral element scheme for problem (2.2) with  
 159 special initial conditions: solve for  $u_h(t) \in V_0^h$  satisfying

$$160 \quad (2.6) \quad \begin{aligned} \langle u_h^{(2)}, v_h \rangle_h + A_h(u_h, v_h) &= \langle f, v_h \rangle_h, \quad \forall v_h \in V_0^h, \\ u_h(0) &= R_h u_0, \quad u_h^{(1)}(0) = (u_1)_I. \end{aligned}$$

161 **2.2. Notation and basic tools.** We will use the same notation as in [23, 24].

The norm and semi-norms for  $W^{k,p}(\Omega)$  and  $1 \leq p < +\infty$ , with standard modifi-  
 cation for  $p = +\infty$  can be defined as follows,

$$\|u\|_{k,p,\Omega} = \left( \sum_{i+j \leq k} \iint_{\Omega} |\partial_x^i \partial_y^j u(x, y)|^p \, dx dy \right)^{1/p},$$

$$|u|_{k,p,\Omega} = \left( \sum_{i+j=k} \iint_{\Omega} |\partial_x^i \partial_y^j u(x,y)|^p dx dy \right)^{1/p}.$$

162 When there is no confusion, for simplicity, sometimes we may use  $\|u\|_k$  and  $|u|_k$  as  
163 norm and semi-norm for  $H^k(\Omega) = W^{k,2}(\Omega)$  respectively.

For any  $v_h \in V^h$ ,  $1 \leq p < +\infty$ , and  $k \geq 1$ , we define the broken Sobolev norms and seminorms by the following symbols,

$$\|v_h\|_{k,p,\Omega} := \left( \sum_e \|v_h\|_{k,p,e}^p \right)^{\frac{1}{p}}, \quad |v_h|_{k,p,\Omega} := \left( \sum_e |v_h|_{k,p,e}^p \right)^{\frac{1}{p}}.$$

164 Let  $Z_{0,e}$  denote the set of  $(k+1) \times (k+1)$  Gauss-Lobatto points of the cell  $e$   
165 and  $Z_0 = \bigcup_e Z_{0,e}$  denote all Gauss-Lobatto points in the mesh  $\Omega_h$ . Let  $\|u\|_{L^2(\Omega)}$  and  
166  $\|u\|_{L^\infty(\Omega)}$  denote the discrete 2-norm and the maximum norm over  $Z_0$  respectively as

$$167 \quad \|u\|_{L^2(\Omega)} = \left[ h^2 \sum_{(x,y) \in Z_0} |u(x,y)|^2 \right]^{\frac{1}{2}}, \quad \|u\|_{L^\infty(\Omega)} = \max_{(x,y) \in Z_0} |u(x,y)|.$$

168 When there is no confusion, for simplicity, sometimes we may use  $\|u\|_{L^2}$  and  $|u|_{L^\infty}$   
169 to denote  $\|u\|_{L^2(\Omega)}$  and  $\|u\|_{L^\infty(\Omega)}$  respectively. For a continuous function  $f(x,y)$ , let  
170  $f_I(x,y)$  denote its piecewise  $Q^k$  Lagrange interpolant at  $Z_{0,e}$  on each cell  $e$ , i.e.,  
171  $f_I \in V^h$  satisfies:

$$172 \quad f(x,y) = f_I(x,y), \quad \forall (x,y) \in Z_0.$$

173 Let  $(f,v)_e$  denote the inner product in  $L^2(e)$  and  $(f,v)$  denotes the inner product  
174 in  $L^2(\Omega)$  as

$$175 \quad (f,v)_e = \iint_e f v dx dy, \quad (f,v) = \iint_{\Omega} f v dx dy = \sum_e (f,v)_e.$$

176 Let  $\langle f,v \rangle_h$  denote the approximation to  $(f,v)$  by using  $(k+1) \times (k+1)$ -point Gauss-  
177 Lobatto quadrature for integration over each cell  $e$ . Then for  $k \geq 2$ , the  $(k+1) \times (k+1)$   
178 Gauss-Lobatto quadrature is exact for integration of tensor product polynomials of  
179 degree  $2k-1 \geq k+1$  on  $\hat{K}$ .

180 We denote  $A^*(\cdot, \cdot)$  as the adjoint bilinear form of  $A(\cdot, \cdot)$  such that

$$181 \quad A^*(v,u) = A(u,v) = (\mathbf{a} \nabla u, \nabla v) + (\mathbf{b} \cdot \nabla u, v) + (cu, v).$$

182 Let superscript  $(i)$  denote  $i$ -th time derivatives for coefficients  $\mathbf{a}$ ,  $\mathbf{b}$ , and  $c$ . For the  
183 time dependent operators  $L$  and  $A$ , the symbols  $L^{(i)}$  and  $A^{(i)}$  are defined as taking  
184 time derivatives only for coefficients:

$$185 \quad L^{(i)}u = -\nabla \cdot (\mathbf{a}^{(i)} \nabla u) + \mathbf{b}^{(i)} \cdot \nabla u + c^{(i)}u,$$

186 and

$$187 \quad A^{(i)}(u,v) = \int_{\Omega} \nabla u^T \mathbf{a}^{(i)} \nabla v + \mathbf{b}^{(i)} \cdot \nabla u + c^{(i)}uv d\mathbf{x}.$$

The symbol  $A_h^{(i)}$  is similarly defined as taking time derivatives only for coefficients in  $A_h$ . With this notation, for  $u(\mathbf{x}, t)$  and time independent test function  $v(\mathbf{x})$ , we have

Leibniz rule

$$(Lu)^{(m)} = \sum_{j=0}^m \binom{m}{j} L^{(m-j)} u^{(j)}, \quad [A(u, v)]^{(m)} = \sum_{j=0}^m \binom{m}{j} A^{(m-j)}(u^{(j)}, v).$$

188 By integration by parts, it is straightforward to verify

$$189 \quad (2.7) \quad (L^{(m-j)} u^{(j)}, v) = A^{(m-j)}(u^{(j)}, v), \quad \forall v \in H_0^1(\Omega).$$

190 There exist constants  $C_i$  ( $i = 1, 2, 3, 4$ ) independent of  $h$  such that  $l^2$ -norm and  
191  $L^2$ -norm are equivalent for  $V^h$ :

$$192 \quad (2.8) \quad \begin{aligned} C_1 \|v_h\|_{l^2} &\leq \|v_h\|_0 \leq C_2 \|v_h\|_{l^2}, \quad \forall v \in V^h, \\ C_3 \langle v_h, v_h \rangle_h &\leq \|v_h\|_0^2 \leq C_4 \langle v_h, v_h \rangle_h, \quad \forall v \in V^h. \end{aligned}$$

193 We have the inverse inequality for polynomials as

$$194 \quad (2.9) \quad \|v_h\|_{k+1, e} \leq Ch^{-1} \|v_h\|_{k, e}, \quad \forall v_h \in V^h, k \geq 0.$$

195 **2.3. Assumption on the coercivity and the elliptic regularity.** For the  
196 operator  $A(u, v) := \int_{\Omega} [\nabla u^T \mathbf{a} \nabla v + (\mathbf{b} \cdot \nabla u)v + cuv] \, d\mathbf{x}$  where  $\mathbf{a} = \begin{pmatrix} a^{11} & a^{12} \\ a^{21} & a^{22} \end{pmatrix}$  is positive  
197 definite and  $\mathbf{b} = [b^1 \quad b^2]$ , assume the coefficients  $a_{ij}, b_j, c \in C^{m_1}([0, T]; W^{m_2, \infty}(\Omega))$   
198 for  $m_1, m_2$  large enough. Thus for  $t \in [0, T]$ ,  $A(u, v) \leq C \|u\|_1 \|v\|_1$  for any  $u, v \in$   
199  $H_0^1(\Omega)$ . As discussed in [24], if we assume  $\lambda_{\mathbf{a}}$  has a positive lower bound and  $\nabla \cdot \mathbf{b} \leq 2c$ ,  
200 where  $\lambda_{\mathbf{a}}$  as the smallest eigenvalues of  $\mathbf{a}$ , the coercivity of the bilinear form can  
201 be easily achieved. For the  $V^h$ -ellipticity, as pointed out in Lemma 5.2 of [24], if  
202  $4\lambda_{\mathbf{a}}c > |\mathbf{b}|^2$ , for  $t \in [0, T]$ ,

$$203 \quad (2.10) \quad C \|v_h\|_1^2 \leq A_h(v_h, v_h), \quad \forall v_h \in V^h,$$

204 can be proven. In the rest of this paper, we assume coercivity for the bilinear forms  
205  $A, A^*$ , and  $A_h$ . We assume the elliptic regularity  $\|w\|_2 \leq C \|f\|_0$  holds for the exact  
206 dual problem of finding  $w \in H_0^1(\Omega)$  satisfying  $A^*(w, v) = (f, v)$ ,  $\forall v \in H_0^1(\Omega)$ . See  
207 [34, 14] for the elliptic regularity with Lipschitz continuous coefficients on a Lipschitz  
208 domain.

209 We remark that in the case of the wave equation we also assume finite speed of  
210 propagation i.e. that there is an upper bound on the eigenvalues of  $\mathbf{a}$ .

211 **3. Quadrature error estimates.** For any continuous function  $u(\mathbf{x}, t_0)$  with  
212 fixed time  $t_0$ , its M-type projection on spatial variables is a continuous piecewise  $Q^k$   
213 polynomial of  $\mathbf{x}$ , denoted as  $u_p(\mathbf{x}, t_0) \in V^h$ . The M-type projection was used to  
214 analyze superconvergence [3]. Detailed definition and some useful properties about  
215 the M-type projection can be also found in [23, 24]. For  $m \geq 0$ ,  $(u_p)^{(m)} = (u^{(m)})_p$ ,  
216 thus there is no ambiguity to use the notation  $u_p^{(m)}$ . The M-type projection has the  
217 following properties. See Theorem 3.2 in [23] for the detailed proof.

218 **THEOREM 3.1.** For  $k \geq 2$ ,

$$219 \quad \|u - u_p\|_{l^2(\Omega)} = \mathcal{O}(h^{k+2}) \|u\|_{k+2}, \quad \forall u \in H^{k+2}(\Omega).$$

$$220 \quad \|u - u_p\|_{l^\infty(\Omega)} = \mathcal{O}(h^{k+2}) \|u\|_{k+2, \infty}, \quad \forall u \in W^{k+2, \infty}(\Omega).$$

222 By applying Bramble-Hilbert Lemma, we have the following standard quadrature  
223 estimates. See [23] for the detailed proof.

LEMMA 3.2. For  $f(\mathbf{x})$ , if  $f(\mathbf{x}) \in H^{k+2}(\Omega)$ , then we have

$$(f, v_h) - \langle f, v_h \rangle_h = \mathcal{O}(h^{k+2}) \|f\|_{k+2} \|v_h\|_2, \quad \forall v_h \in V^h.$$

224 The next lemma shows the superconvergence of the bilinear form with Gauss-  
225 Lobatto quadrature  $A_h$ , and it collects the results of Lemma 4.5 - Lemma 4.8 of  
226 [24].

227 LEMMA 3.3. For  $i, j \geq 0$  and any fixed  $t \in [0, T]$ , assuming sufficiently smooth  
228 coefficients  $\mathbf{a}, \mathbf{b}, c$  and function  $u(\mathbf{x}, t) \in H^{(k+3)}(\Omega)$ , we have

(3.1)

$$229 A_h^{(i)}((u - u_p)^{(j)}, v_h) = \begin{cases} \mathcal{O}(h^{k+2}) \|u^{(j)}(t)\|_{k+3} \|v_h\|_2, & \text{if } v_h \in V_0^h \text{ or } \mathbf{a} \text{ is diagonal;} \\ \mathcal{O}(h^{k+\frac{3}{2}}) \|u^{(j)}(t)\|_{k+3} \|v_h\|_2, & \text{otherwise.} \end{cases}$$

230

231 The following results are Lemma 3.5, Theorem 3.6, Theorem 3.7 in [24].

LEMMA 3.4. If  $f \in H^2(\Omega)$  or  $f \in V^h$ , we have

$$(f, v_h) - \langle f, v_h \rangle_h = \mathcal{O}(h^2) \|f\|_2 \|v_h\|_0, \quad \forall v_h \in V^h.$$

232 LEMMA 3.5. Assume all coefficients of (2.3) are in  $L^\infty([0, T]; W^{2,\infty}(\Omega))$ . We  
233 have

$$234 A(z_h, v_h) - A_h(z_h, v_h) = \mathcal{O}(h) \|v_h\|_2 \|z_h\|_1, \quad \forall v_h, z_h \in V^h.$$

235 LEMMA 3.6. For the differential operator  $L$  and any fixed  $t \in [0, T]$ , assume  
236  $a_{ij}(\mathbf{x}, t), b_i(\mathbf{x}, t), c(\mathbf{x}, t) \in L^\infty([0, T]; W^{k+2,\infty}(\Omega))$  and  $u(\mathbf{x}, t) \in H^{k+3}(\Omega)$ . For  $k \geq 2$ ,  
237 we have

(3.2)

$$238 A(u, v_h) - A_h(u, v_h) = \begin{cases} \mathcal{O}(h^{k+2}) \|u(t)\|_{k+3} \|v_h\|_2, & \text{if } v_h \in V_0^h \text{ or } (\mathbf{a}\nabla u) \cdot \mathbf{n} = 0 \text{ on } \partial\Omega \\ \mathcal{O}(h^{k+\frac{3}{2}}) \|u(t)\|_{k+3} \|v_h\|_2, & \text{otherwise} \end{cases},$$

239

240 where  $\mathbf{n}$  denotes the unit vector normal to the domain boundary  $\partial\Omega$ .

241 REMARK 3.7. There is half order loss in (3.1), only when using  $v \in V^h$  for non-  
242 diagonal  $\mathbf{a}$ , i.e., when solving second order equations containing mixed second order  
243 derivatives with homogeneous Neumann boundary conditions. See [22] for detailed  
244 proof of (3.2) for the homogeneous Neumann boundary condition case, i.e.,  $(\mathbf{a}\nabla u) \cdot \mathbf{n} =$   
245  $0$  along the domain boundary.

246 We have the Gronwall's inequality in integral form as follows:

247 LEMMA 3.8. Let  $\xi(t)$  be continuous on  $[0, T]$  and

$$248 \xi(t) \leq C_1 \int_0^t \xi(s) ds + \alpha(t)$$

249 for constant  $C_1 \geq 0$  and  $\alpha(t) \geq 0$  nondecreasing in  $t$ . Then  $\xi(t) \leq \alpha(t)e^{C_1 t}$  thus  
250  $\xi(t) \leq \alpha(t)e^{C_1 T} = C\alpha(t)$  for all  $0 \leq t \leq T$ .

**4. Error estimates for the elliptic projection.** Let  $u_h(\mathbf{x}, t)$  denote the solution of the semi-discrete numerical scheme. Let  $e(\mathbf{x}, t) = u_h(\mathbf{x}, t) - u_p(\mathbf{x}, t)$ , then we can write

$$e = \theta_h + \rho_h,$$

251 where  $\theta_h := u_h - R_h u \in V_0^h$  and  $\rho_h := R_h u - u_p \in V_0^h$ .

252 In this section, we will establish the superconvergence result for the elliptic projec-  
253 tion, which is an important step for proving the superconvergence of function values.

254 We have the following superconvergence result for  $\|\rho_h^{(m)}(t)\|$ ,  $m \geq 0$ ,  $t \in [0, T]$ .

255 **LEMMA 4.1.** *If  $a_{ij}$ ,  $b_j$ ,  $c \in C^m([0, T]; W^{k+2, \infty}(\Omega))$ ,  $u \in C^m([0, T]; H^{k+4}(\Omega))$ ,  
256 then we have*

$$257 \quad (4.1) \quad \|\rho_h^{(m)}(t)\|_1 \leq Ch^{k+1} \sum_{j=0}^m (\|u^{(j)}(t)\|_{k+3} + \|(Lu)^{(j)}(t)\|_{k+2}),$$

(4.2)

$$258 \quad \|\rho_h^{(m)}\|_{L^2([0, T]; L^2(\Omega))} \leq Ch^{k+2} \sum_{j=0}^m (\|u^{(j)}\|_{L^2([0, T]; H^{k+3}(\Omega))} + \|(Lu)^{(j)}\|_{L^2([0, T]; H^{k+2}(\Omega))}),$$

259

260

(4.3)

$$261 \quad \|\rho_h^{(m)}\|_{L^\infty([0, T]; L^2(\Omega))} \leq Ch^{k+2} \sum_{j=0}^m (\|u^{(j)}\|_{L^\infty([0, T]; H^{k+3}(\Omega))} + \|(Lu)^{(j)}\|_{L^\infty([0, T]; H^{k+2}(\Omega))})$$

262 where  $C$  is independent of  $h$ ,  $u$ ,  $f$ , and time  $t$ .

263 *Proof.* First we prove (4.1), with which we then prove (4.2) and (4.3) by the dual  
264 argument.

265 From the definition of the discrete elliptic projection (2.4) we have

$$266 \quad (4.4) \quad A_h(\rho_h, v_h) = \epsilon(v_h), \quad \forall v_h \in V_0^h.$$

268 where

$$269 \quad \epsilon(v_h) = \langle -Lu, v_h \rangle_h - A_h(u_p, v_h).$$

270 Note that  $v_h$  is time independent. Taking  $m$  time derivatives of (4.4) yields

$$271 \quad (4.5) \quad (A_h(\rho_h, v_h))^{(m)} = \sum_{j=0}^m \binom{m}{j} A_h^{(m-j)}(\rho_h^{(j)}, v_h) = \epsilon^{(m)}(v_h).$$

272 The term  $\epsilon^{(m)}(v_h)$  can be rewritten as follows:

$$273 \quad \begin{aligned} \epsilon^{(m)}(v_h) &= \langle (Lu)^{(m)}, v_h \rangle_h - (A_h(u_p, v_h))^{(m)} \\ &= \left[ \langle (Lu)^{(m)}, v_h \rangle - (A(u, v_h))^{(m)} \right] - \left[ \langle (Lu)^{(m)}, v_h \rangle - \langle (Lu)^{(m)}, v_h \rangle_h \right] \\ &\quad + \left[ (A(u, v_h))^{(m)} - (A_h(u, v_h))^{(m)} \right] + (A_h(u - u_p, v_h))^{(m)}. \end{aligned}$$

274 By Leibniz rule and (2.7), we have

$$275 \quad \langle (Lu)^{(m)}, v_h \rangle - (A(u, v_h))^{(m)} = \sum_{j=0}^m \binom{m}{j} \left[ (L^{(m-j)} u^{(j)}, v_h) - A^{(m-j)}(u^{(j)}, v_h) \right] = 0.$$

276 By Lemma 3.2,

$$277 \quad \langle (Lu)^{(m)}, v_h \rangle - \langle (Lu)^{(m)}, v_h \rangle_h = \mathcal{O}(h^{k+2}) \|(Lu)^{(m)}(t)\|_{k+2} \|v_h\|_2.$$



278 By Leibniz rule and Lemma 3.6,

$$\begin{aligned}
279 \quad (A(u, v_h))^{(m)} - (A_h(u, v_h))^{(m)} &= \sum_{j=0}^m \binom{m}{j} \left[ A^{(m-j)}(u^{(j)}, v_h) - A_h^{(m-j)}(u^{(j)}, v_h) \right] \\
280 \quad &= \mathcal{O}(h^{k+2}) \sum_{j=0}^m \binom{m}{j} \|u^{(j)}(t)\|_{k+3} \|v_h\|_2. \\
281
\end{aligned}$$

282 Now, Lemma 3.3 implies

$$\begin{aligned}
283 \quad (A_h(u - u_p, v_h))^{(m)} &= \sum_{j=0}^m \binom{m}{j} A_h^{(m-j)} \left( (u - u_p)^{(j)}, v_h \right) \\
284 \quad &= \mathcal{O}(h^{k+2}) \sum_{j=0}^m \binom{m}{j} \|u^{(j)}(t)\|_{k+3} \|v_h\|_2. \\
285
\end{aligned}$$

286 Thus we have

$$287 \quad (4.6) \quad \epsilon^{(m)}(v_h) = \mathcal{O}(h^{k+2}) \left( \sum_{j=0}^m \|u^{(j)}(t)\|_{k+3} + \|(Lu)^{(m)}(t)\|_{k+2} \right) \|v_h\|_2.$$

288 For  $i \geq 0$ , by the  $V_h$ -ellipticity (2.10), (4.5), and (4.6) we have

$$\begin{aligned}
& C \|\rho_h^{(i)}(t)\|_1^2 \leq A_h(\rho_h^{(i)}, \rho_h^{(i)}) \\
&= \sum_{j=0}^i \binom{i}{j} A_h^{(i-j)}(\rho_h^{(j)}, \rho_h^{(i)}) - \sum_{j=0}^{i-1} \binom{i}{j} A_h^{(i-j)}(\rho_h^{(j)}, \rho_h^{(i)}) \\
289 \quad &= \epsilon^{(i)}(\rho_h^{(i)}) - \sum_{j=0}^{i-1} \binom{i}{j} A_h^{(i-j)}(\rho_h^{(j)}, \rho_h^{(i)}) \\
&\leq \mathcal{O}(h^{k+1}) \left( \sum_{j=0}^i \|u^{(j)}\|_{k+3} + \|(Lu)^{(i)}\|_{k+2} \right) h \|\rho_h^{(i)}\|_2 + C \sum_{j=0}^{i-1} \|\rho_h^{(j)}(t)\|_1 \|\rho_h^{(i)}(t)\|_1 \\
&\leq \left[ \mathcal{O}(h^{k+1}) \left( \sum_{j=0}^i \|u^{(j)}\|_{k+3} + \|(Lu)^{(i)}\|_{k+2} \right) + C \sum_{j=0}^{i-1} \|\rho_h^{(j)}(t)\|_1 \right] \|\rho_h^{(i)}(t)\|_1,
\end{aligned}$$

290 the last inequality follows from an application of an inverse estimate. Thus

$$291 \quad (4.7) \quad \|\rho_h^{(i)}(t)\|_1 \leq \mathcal{O}(h^{k+1}) \left( \sum_{j=0}^i \|u^{(j)}\|_{k+3} + \|(Lu)^{(i)}\|_{k+2} \right) + C \sum_{j=0}^{i-1} \|\rho_h^{(j)}(t)\|_1.$$

292 Now (4.1) can be proven by induction as follows. First, set  $i = 0$  in (4.7) to obtain  
293 (4.1) with  $m = 0$ . Second, assume (4.7) holds for  $m = i - 1$ , then (4.7) implies that  
294 (4.1) also holds for  $m = i$ .

295 For fixed  $t \in [0, T]$ , to estimate  $\rho_h^{(m)}$  in  $L^2$ -norm, we consider the dual problem:  
296 find  $\phi_h \in V_0^h$  satisfying: for  $i \geq 0$ ,

$$297 \quad (4.8) \quad A^*(\phi_h, v_h) = (\rho_h^{(i)}(t), v_h), \quad \forall v_h \in V_0^h.$$

298 Based on Theorem 5.3 in [24], by assuming the elliptic regularity and  $V^h$  ellipticity,  
299 problem (4.8) has a unique solution satisfying

$$300 \quad (4.9) \quad \|\phi_h\|_2 \leq C \|\rho_h^{(i)}(t)\|_0.$$

301 Take  $v_h = \rho_h^{(i)}$  in (4.8) then we have

$$\begin{aligned} 302 \quad & \|\rho_h^{(i)}(t)\|_0^2 \\ 303 \quad & = A^*(\phi_h, \rho_h^{(i)}) = A(\rho_h^{(i)}, \phi_h) \\ 304 \quad & = \sum_{j=0}^i \binom{i}{j} A^{(i-j)}(\rho_h^{(j)}, \phi_h) - \sum_{j=0}^{i-1} \binom{i}{j} A^{(i-j)}(\rho_h^{(j)}, \phi_h) \\ 305 \quad & = \sum_{j=0}^i \binom{i}{j} \left( A_h^{(i-j)}(\rho_h^{(j)}, \phi_h) + E \left( A^{(i-j)}(\rho_h^{(j)}, \phi_h) \right) \right) - \sum_{j=0}^{i-1} \binom{i}{j} \left( \rho_h^{(j)}, (L^*)^{(i-j)} \phi_h \right). \\ 306 \end{aligned}$$

307 Note that  $\forall \chi \in V_0^h$ , with (4.5) and (4.6),  
(4.10)

$$\begin{aligned} & \sum_{j=0}^i \binom{i}{j} A_h^{(i-j)}(\rho_h^{(j)}, \phi_h) \\ & = \sum_{j=0}^i \binom{i}{j} A_h^{(i-j)}(\rho_h^{(j)}, \phi_h - \chi) + \sum_{j=0}^i \binom{i}{j} A_h^{(i-j)}(\rho_h^{(j)}, \chi) \\ 308 \quad & = \sum_{j=0}^i \binom{i}{j} A_h^{(i-j)}(\rho_h^{(j)}, \phi_h - \chi) + \epsilon^{(i)}(\chi) \\ & \leq C \sum_{j=0}^i \|\rho_h^{(j)}(t)\|_1 \|\phi_h - \chi\|_1 + \mathcal{O}(h^{k+2}) \left( \sum_{j=0}^i \|u^{(j)}(t)\|_{k+3} + \|(Lu)^{(i)}(t)\|_{k+2} \right) \|\chi\|_2. \end{aligned}$$

309 Let  $\chi = \Pi_1 \phi_h$  where  $\Pi_1$  is the  $L^2$  projection to functions in the continuous  
310 piecewise  $Q^1$  polynomial space, see [24]. Then we have  $\|\phi_h - \chi\|_1 \leq Ch \|\phi_h\|_2$  and  
311  $\|\chi\|_2 \leq C \|\phi_h\|_2$ . Inserting (4.1) and (4.9) into (4.10), we have  
(4.11)

$$312 \quad \sum_{j=0}^i \binom{i}{j} A_h^{(i-j)}(\rho_h^{(j)}, \phi_h) = \mathcal{O}(h^{k+2}) \left( \sum_{j=0}^i (\|u^{(j)}(t)\|_{k+3} + \|(Lu)^{(i)}(t)\|_{k+2}) \right) \|\phi_h\|_2.$$

313 Thus with (4.11), Lemma 3.6, and inverse inequality we have

$$\begin{aligned}
& \|\rho_h^{(i)}(t)\|_0^2 \\
& \leq \mathcal{O}(h^{k+2}) \left( \sum_{j=0}^i \|u^{(j)}(t)\|_{k+3} + \|(Lu)^{(i)}(t)\|_{k+2} \right) \|\phi_h\|_2 \\
& \quad + \mathcal{O}(h^{k+2}) \sum_{j=0}^i \|\rho_h^{(j)}(t)\|_{k+2} \|\phi_h\|_2 + C \sum_{j=0}^{i-1} \|\rho_h^{(j)}(t)\|_0 \|\phi_h\|_2 \\
314 \quad (4.12) \quad & = \left[ \mathcal{O}(h^{k+2}) \left( \sum_{j=0}^i \|u^{(j)}\|_{k+3} + \|(Lu)^{(i)}\|_{k+2} \right) + C \sum_{j=0}^{i-1} \|\rho_h^{(j)}(t)\|_0 \right] \|\phi_h\|_2 \\
& \leq \left( \mathcal{O}(h^{k+2}) \left( \sum_{j=0}^i \|u^{(j)}\|_{k+3} + \|(Lu)^{(i)}\|_{k+2} \right) + C \sum_{j=0}^{i-1} \|\rho_h^{(j)}(t)\|_0 \right) \|\rho_h^{(i)}(t)\|_0,
\end{aligned}$$

315 where (4.9) is applied in the last inequality.

316 With similar induction arguments as above, (4.12) implies

$$317 \quad (4.13) \quad \|\rho_h^{(i)}(t)\|_0 \leq \mathcal{O}(h^{k+2}) \sum_{j=0}^i (\|u^{(j)}(t)\|_{k+3} + \|(Lu)^{(j)}(t)\|_{k+2}).$$

318 Take the square for both sides of (4.13) then integrate from 0 to  $T$  and take the  
319 square root for both sides, we can get (4.2). Take the maximum of the right hand  
320 side then the left hand side of (4.13) for  $t \in [0, T]$ , we can get (4.3).  $\square$

321 **5. Accuracy of the semi-discrete schemes.** In this section, we will prove  
322 the  $(k+2)$ -th order of accuracy of  $Q^k$  spectral element method, when the errors are  
323 measured only at nodes of degree of freedoms, which is a superconvergence result of  
324 function values.

325 Throughout this section the generic constant  $C$  is independent of  $h$ . Although in  
326 principle it may depend on  $t$  though the coefficients  $a_{ij}(t)$ ,  $b_j(t)$ ,  $c(t)$ , we also treat  
327 it as independent of time since its time dependent version can always be replaced by  
328 a time independent constant after taking maximum over the ime interval  $[0, T]$ . In  
329 what follows we will state and prove the main theorems for wave, parabolic and the  
330 Schrödinger equations.

331 **5.1. The hyperbolic problem.** The main result for the wave equation can be  
332 stated as the following theorem.

333 **THEOREM 5.1.** *If  $a_{ij}$ ,  $b_j$ ,  $c \in C^2([0, T]; W^{k+2, \infty}(\Omega))$ ,  $u \in C^2([0, T]; H^{k+4}(\Omega))$ ,*  
334 *then for the semi-discrete scheme (2.6) for the problem (2.2), we have*

$$\begin{aligned}
& \|u_h - u\|_{L^2([0, T]; l^2(\Omega))} \leq Ch^{k+2} \left( \sum_{j=0}^2 (\|u^{(j)}\|_{L^2([0, T]; H^{k+3}(\Omega))} + \|(Lu)^{(j)}\|_{L^2([0, T]; H^{k+2}(\Omega))}) \right. \\
335 & \quad \left. + \sum_{j=0}^1 (\|u^{(j)}(0)\|_{k+3} + \|(Lu)^{(j)}(0)\|_{k+2}) \right), \\
& \|u_h - u\|_{L^\infty([0, T]; l^2(\Omega))} \leq Ch^{k+2} \sum_{j=0}^2 (\|u^{(j)}\|_{L^\infty([0, T]; H^{k+3}(\Omega))} + \|(Lu)^{(j)}\|_{L^\infty([0, T]; H^{k+2}(\Omega))}),
\end{aligned}$$

336 where  $C$  is independent of  $t$ ,  $h$ ,  $u$ , and  $f$ .

337 *Proof.* Note that for the numerical solution  $u_h$  we have

$$338 \quad (5.1) \quad \langle u_h^{(2)}, v_h \rangle_h + A_h(u_h, v_h) = \langle f, v_h \rangle_h, \quad \forall v_h \in V_0^h.$$

339 The exact solution  $u$  satisfies  $u_{tt} = -Lu + f$  thus the elliptic projection (2.4) satisfies

$$340 \quad A_h(R_h u, v_h) = \langle u^{(2)} - f, v_h \rangle_h, \quad \forall v_h \in V_0^h.$$

341 Subtracting the two equations above, we get  $\theta_h = u_h - R_h u$ , which satisfies

$$342 \quad (5.2) \quad \langle \theta_h^{(2)}, v_h \rangle_h + A_h(\theta_h, v_h) = -\langle \rho_h^{(2)}, v_h \rangle_h + \langle u^{(2)} - u_p^{(2)}, v_h \rangle_h, \quad \forall v_h \in V_0^h.$$

343 Note that

$$344 \quad (5.3) \quad \frac{d}{dt} A_h(\theta_h, \theta_h) = A_h^{(1)}(\theta_h, \theta_h) + 2A_h(\theta_h, \theta_h^{(1)}) - \langle \mathbf{b} \cdot \nabla \theta_h, \theta_h^{(1)} \rangle_h + \langle \mathbf{b} \cdot \nabla \theta_h^{(1)}, \theta_h \rangle_h.$$

346 Thus by Lemma 3.4 and (2.8), we have

$$347 \quad (5.4) \quad \begin{aligned} \langle \mathbf{b} \cdot \nabla \theta_h^{(1)}, \theta_h \rangle_h &= \langle \mathbf{b} \cdot \nabla \theta_h^{(1)}, \theta_h \rangle_h + \mathcal{O}(h^2) |\mathbf{b} \theta_h|_2 \|\nabla \theta_h^{(1)}\|_0 \\ &\leq \langle \mathbf{b} \cdot \nabla \theta_h^{(1)}, \theta_h \rangle_h + C \|\theta_h^{(1)}\|_0 \|\theta_h\|_1 \\ &= \langle \nabla \cdot (\mathbf{b} \theta_h), \theta_h^{(1)} \rangle_h + C \|\theta_h^{(1)}\|_0 \|\theta_h\|_1 \\ &\leq C \|\theta_h^{(1)}\|_0 \|\theta_h\|_1 \leq C \|\theta_h^{(1)}\|_{l^2} \|\theta_h\|_1, \end{aligned}$$

348 where an inverse inequality was applied to the first inequality and integration by parts  
349 in  $\theta_h \in V_0^h$  yields the last equation.

350 Next we estimate  $\|\theta_h^{(1)}(s)\|_0^2 + \|\theta_h(s)\|_1^2$ . Take  $v_h = \theta_h^{(1)}$  in (5.2) and integrate  
351 with respect to  $t$  from 0 to  $s$ . With (5.3), we have

$$352 \quad (5.5) \quad \begin{aligned} &\int_0^s \frac{d}{dt} \left( \frac{1}{2} \langle \theta_h^{(1)}, \theta_h^{(1)} \rangle_h + \frac{1}{2} A_h(\theta_h, \theta_h) \right) dt \\ &= \frac{1}{2} \int_0^s A_h^{(1)}(\theta_h, \theta_h) - \langle \mathbf{b} \cdot \nabla \theta_h, \theta_h^{(1)} \rangle_h + \langle \mathbf{b} \cdot \nabla \theta_h^{(1)}, \theta_h \rangle_h - 2 \langle \rho_h^{(2)}, \theta_h^{(1)} \rangle_h + 2 \langle u^{(2)} - u_p^{(2)}, \theta_h^{(1)} \rangle_h dt. \end{aligned}$$

353 With  $\theta_h(0) = 0$  and (5.4), this implies

$$354 \quad (5.6) \quad \begin{aligned} &\frac{1}{2} (\|\theta_h^{(1)}(s)\|_{l^2}^2 + A_h(\theta_h(s), \theta_h(s))) - \frac{1}{2} \|\theta_h^{(1)}(0)\|_{l^2}^2 \\ &\leq C \int_0^s (\|\theta_h\|_1^2 + \|\theta_h^{(1)}\|_0 \|\theta_h\|_1) dt + C \int_0^s \|\rho_h^{(2)}\|_0 \|\theta_h^{(1)}\|_0 dt \\ &\quad + C \int_0^s \|u^{(2)} - u_p^{(2)}\|_{l^2} \|\theta_h^{(1)}\|_0 dt \\ &\leq C \int_0^s (\|\theta_h^{(1)}\|_0^2 + \|\theta_h\|_1^2) dt + C \int_0^s (\|\rho_h^{(2)}\|_0^2 + \|u^{(2)} - u_p^{(2)}\|_{l^2}^2) dt, \end{aligned}$$

355 where Cauchy-Schwarz inequality was used in the last inequality.

356 Thus with (2.8), (2.10), and (5.6) we have

$$357 \quad (5.7) \quad \begin{aligned} &\|\theta_h^{(1)}(s)\|_0^2 + \|\theta_h(s)\|_1^2 \leq C \|\theta_h^{(1)}(s)\|_{l^2}^2 + C A_h(\theta_h(s), \theta_h(s)) \\ &\leq C \|\theta_h^{(1)}(0)\|_{l^2}^2 + C \int_0^s (\|\theta_h^{(1)}\|_0^2 + \|\theta_h\|_1^2) dt + C \int_0^s (\|\rho_h^{(2)}\|_0^2 + \|u^{(2)} - u_p^{(2)}\|_{l^2}^2) dt. \end{aligned}$$

358 With the Gronwall inequality (3.8) we can eliminate the second term to find

$$359 \quad \|\theta_h^{(1)}(s)\|_0^2 + \|\theta_h(s)\|_1^2 \leq C\|\theta_h^{(1)}(0)\|_{l^2}^2 + C \int_0^s \|\rho_h^{(2)}\|_0^2 + \|u^{(2)} - u_p^{(2)}\|_{l^2}^2 dt.$$

361 With (4.3) and Theorem 3.1 we have

$$362 \quad \|\theta_h^{(1)}(s)\|_0^2 + \|\theta_h(s)\|_1^2 \leq C\|\theta_h^{(1)}(0)\|_{l^2}^2 + \mathcal{O}(h^{2k+4}) \int_0^s \sum_{j=0}^2 (\|u^{(j)}\|_{k+3} + \|(Lu)^{(j)}\|_{k+2})^2 dt,$$

363 i.e.

(5.8)

$$364 \quad \|\theta_h^{(1)}(s)\|_0 + \|\theta_h(s)\|_1 \leq C\|\theta_h^{(1)}(0)\|_{l^2} + \mathcal{O}(h^{k+2}) \int_0^s \sum_{j=0}^2 (\|u^{(j)}\|_{k+3} + \|(Lu)^{(j)}\|_{k+2}) dt.$$

365 To estimate  $\|\theta_h^{(1)}(0)\|_{l^2}$  we use Theorem 3.1, (4.3), and (2.8),

$$\begin{aligned} 366 \quad \|\theta_h^{(1)}(0)\|_{l^2} &= \|(u_1)_I - (R_h u)^{(1)}(0)\|_{l^2} \\ 367 \quad &= \|(u_1)_I - (u_1)_p + (u_1)_p - (R_h u)^{(1)}(0)\|_{l^2} \\ 368 \quad &\leq \|(u_1)_I - (u_1)_p\|_{l^2} + \|(u_1)_p - (R_h u)^{(1)}(0)\|_{l^2} \\ 369 \quad &= \|u_1 - (u_1)_p\|_{l^2} + \|(u_1)_p - R_h(u^{(1)}(0))\|_{l^2} \\ 370 \quad &= \|u_1 - (u_1)_p\|_{l^2} + \|(u_1)_p - R_h(u_1)\|_{l^2} \\ 371 \quad &= \mathcal{O}(h^{k+2})(\|u_1\|_{k+3} + \|Lu_1\|_{k+2}). \end{aligned}$$

373 Then we have

$$374 \quad (5.9) \quad \|\theta_h^{(1)}\|_0 + \|\theta_h\|_1 \leq \mathcal{O}(h^{k+2}) \left( \|u_1\|_{k+3} + \|Lu_1\|_{k+2} + \int_0^s \sum_{j=0}^2 (\|u^{(j)}\|_{k+3} + \|(Lu)^{(j)}\|_{k+2}) dt \right).$$

375 Now with (4.2), (4.3), and Theorem 3.1, the proof is concluded.  $\square$

376 **5.2. The parabolic problem.** We now present the main result for the parabolic  
377 problem.

378 **THEOREM 5.2.** *If  $a_{ij}, b_j, c \in C^1([0, T]; W^{k+1, \infty}(\Omega))$ ,  $u \in C^1([0, T]; H^{k+4}(\Omega))$ ,*  
379 *then for the semi-discrete scheme (2.5) for problem (2.1), we have*

$$\begin{aligned} 380 \quad \|u_h - u\|_{L^2([0, T]; l^2(\Omega))} &\leq Ch^{k+2} \sum_{j=0}^1 (\|u^{(j)}\|_{L^2([0, T]; H^{k+3}(\Omega))} + \|(Lu)^{(j)}\|_{L^2([0, T]; H^{k+2}(\Omega))}), \\ \|u_h - u\|_{L^\infty([0, T]; l^2(\Omega))} &\leq Ch^{k+2} \sum_{j=0}^1 (\|u^{(j)}\|_{L^\infty([0, T]; H^{k+3}(\Omega))} + \|(Lu)^{(j)}\|_{L^\infty([0, T]; H^{k+2}(\Omega))}), \end{aligned}$$

381 where  $C$  is independent of  $t, h, u$ , and  $f$ .

382 *Proof.* By our semi-discrete numerical scheme (2.5) and the definition of the el-  
383 liptic projection (2.4), we have

$$384 \quad (5.10) \quad \langle \theta_h^{(1)}, v_h \rangle_h + A_h(\theta_h, v_h) = -\langle \rho_h^{(1)}, v_h \rangle_h + \langle u^{(1)} - u_p^{(1)}, v_h \rangle, \quad \forall v_h \in V_0^h.$$

385 Take  $v_h = \theta_h^{(1)}$  in (5.10) and integrate with respect to  $t$  from 0 to  $s$ ,

$$(5.11) \quad \int_0^s \langle \theta_h^{(1)}, \theta_h^{(1)} \rangle_h + \frac{1}{2} \frac{d}{dt} A_h(\theta_h, \theta_h) dt$$

$$386 = \frac{1}{2} \int_0^s A_h^{(1)}(\theta_h, \theta_h) - \langle \mathbf{b} \cdot \nabla \theta_h, \theta_h^{(1)} \rangle_h + \langle \mathbf{b} \cdot \nabla \theta_h^{(1)}, \theta_h \rangle_h - 2 \langle \rho_h^{(1)}, \theta_h^{(1)} \rangle_h + 2 \langle u^{(1)} - u_p^{(1)}, \theta_h^{(1)} \rangle_h dt.$$

387 Note that  $\theta_h(0) = 0$ , then with (2.8), (5.4), and (5.11) we have

$$\int_0^s \langle \theta_h^{(1)}, \theta_h^{(1)} \rangle_h dt + \|\theta_h(s)\|_1^2 \leq \int_0^s \langle \theta_h^{(1)}, \theta_h^{(1)} \rangle_h dt + C A_h(\theta_h(s), \theta_h(s))$$

$$\leq C \int_0^s \|\theta_h\|_1^2 dt + C \int_0^s \|\theta_h^{(1)}\|_{l^2} \|\theta_h\|_1 dt + C \int_0^s \|\rho_h^{(1)}\|_{l^2} \|\theta_h^{(1)}\|_{l^2} dt$$

$$388 + C \int_0^s \|u^{(1)} - u_p^{(1)}\|_{l^2} \|\theta_h^{(1)}\|_{l^2} dt$$

$$\leq C \int_0^s \|\theta_h\|_1^2 dt + \int_0^s \epsilon \langle \theta_h^{(1)}, \theta_h^{(1)} \rangle_h + \frac{C}{4\epsilon} \|\theta_h\|_1^2 dt + \int_0^s \epsilon \langle \theta_h^{(1)}, \theta_h^{(1)} \rangle_h + \frac{C}{4\epsilon} \|\rho_h^{(1)}\|_0^2 dt$$

$$+ \int_0^s \epsilon \langle \theta_h^{(1)}, \theta_h^{(1)} \rangle_h + \frac{C}{4\epsilon} \|u^{(1)} - u_p^{(1)}\|_{l^2}^2 dt,$$

389 where Cauchy-Schwartz inequality was applied in the last inequality. Thus we have

$$(1 - 3\epsilon) \int_0^s \langle \theta_h^{(1)}, \theta_h^{(1)} \rangle_h dt + \|\theta_h(s)\|_1^2 \leq C \left(1 + \frac{1}{4\epsilon}\right) \int_0^s \|\theta_h\|_1^2 dt + \frac{C}{4\epsilon} \int_0^s \|\rho_h^{(1)}\|_0^2 dt$$

$$390 + \frac{C}{4\epsilon} \int_0^s \|u^{(1)} - u_p^{(1)}\|_{l^2}^2 dt.$$

391 Now take  $\epsilon$  small enough to make  $1 - 3\epsilon \geq \frac{1}{2}$  then

$$(5.12) \quad \frac{1}{2} \int_0^s \langle \theta_h^{(1)}(s), \theta_h^{(1)}(s) \rangle_h dt + \|\theta_h(s)\|_1^2 \leq C \int_0^s \|\rho_h^{(1)}\|_0^2 dt + C \int_0^s \|u^{(1)} - u_p^{(1)}\|_{l^2}^2 dt$$

$$392 + C \int_0^s \left( \|\theta_h(t)\|_1^2 + \frac{1}{2} \int_0^t \langle \theta_h^{(1)}(\eta), \theta_h^{(1)}(\eta) \rangle_h d\eta \right) dt.$$

393 Next, apply Gronwall's inequality to eliminate the last term of the right hand side of  
394 (5.12) to find

$$395 \quad \frac{1}{2} \int_0^s \langle \theta_h^{(1)}, \theta_h^{(1)} \rangle_h dt + \|\theta_h\|_1^2 \leq C \int_0^s \|\rho_h^{(1)}\|_0^2 dt + C \int_0^s \|u^{(1)} - u_p^{(1)}\|_{l^2}^2 dt.$$

396 Using (4.2), (4.3), and Theorem 3.1 we have

$$397 \quad \frac{1}{2} \int_0^s \langle \theta_h^{(1)}, \theta_h^{(1)} \rangle_h dt + \|\theta_h\|_1^2 \leq \mathcal{O}(h^{k+2}) \int_0^s \sum_{j=0}^1 (\|u^{(j)}\|_{k+3} + \|(Lu)^{(j)}\|_{k+2}) dt,$$

$$398$$

399 concluding the proof.  $\square$

400 **5.3. The linear Schrödinger equation.** Consider the problem

$$401 \quad (5.13) \quad \begin{cases} iu_t = -\Delta u + Vu + f, & \text{in } \Omega \times [0, T], \\ u(\mathbf{x}, t) = 0, & \text{on } \partial\Omega \times [0, T], \\ u(\mathbf{x}, 0) = u_0(\mathbf{x}), & \text{in } \Omega, \end{cases}$$

402 where  $\Omega \in R^2$  is a rectangular domain, the functions  $u_0(\mathbf{x})$ ,  $f(\mathbf{x}, t)$ , and the solution  
 403  $u(\mathbf{x}, t)$  are complex-valued while the potential function  $V(\mathbf{x}, t)$  is real-valued, non-  
 404 negative, and bounded for all  $(\mathbf{x}, t) \in \Omega \times [0, T]$ .

In this subsection we work with complex-valued functions and the definition of  
 inner product and the induced norms are modified accordingly. For instance, for  
 complex-valued  $v, w \in L^2(\Omega)$ , the inner product is defined as

$$(v, w) := \int_{\Omega} v \bar{w} d\mathbf{x}.$$

405 We assume all the functions of the function spaces defined previously are complex-  
 406 valued for this subsection, such as  $H^k(\Omega)$ ,  $H_0^k(\Omega)$ ,  $V_0^h$ , etc.

407 The variational form of (5.13) is: for  $t \in [0, T]$ , find  $u(t) \in H_0^1(\Omega)$  satisfying:

$$408 \quad (5.14) \quad \begin{cases} i(u_t, v) - (\nabla u, \nabla v) - (Vu, v) = (f, v), & \forall v \in H_0^1(\Omega), \\ u(0) = u_0, & \forall v \in H_0^1(\Omega). \end{cases}$$

409 The semi-discrete numerical scheme discretizing (5.14) is to find  $u_h \in V_0^h$  satisfying

$$410 \quad (5.15) \quad \begin{cases} i\langle (u_h)_t, v_h \rangle_h - \langle \nabla u_h, \nabla v_h \rangle_h - \langle Vu_h, v_h \rangle_h = \langle f, v_h \rangle_h, & \forall v_h \in V_0^h, \\ u_h(0) = (u_0)_I, \end{cases}$$

411 and the elliptic projection  $R_h u \in V_0^h$  is defined as

$$412 \quad (5.16) \quad \langle \nabla R_h u, \nabla v_h \rangle_h + \langle VR_h u, v_h \rangle_h = \langle -\Delta u + Vu, v_h \rangle_h, \quad \forall v_h \in V_0^h.$$

As in Section 4, we split the error into two parts

$$e = \theta_h + \rho_h,$$

413 where  $\theta_h = u_h - R_h u \in V_0^h$  and  $\rho_h = R_h u - u_p \in V_0^h$ . The estimates for  $\rho_h^{(m)}$ ,  $m \geq 0$   
 414 from Lemma 4.1 are still valid.

415 **THEOREM 5.3.** *If  $u \in C^1([0, T]; H^{k+4}(\Omega))$ , then for the semi-discrete scheme*  
 416 *(5.15) for problem (5.13), we have*

$$417 \quad \begin{aligned} \|u_h - u\|_{L^2([0, T]; L^2(\Omega))} &\leq Ch^{k+2} \sum_{j=0}^1 (\|u^{(j)}\|_{L^2([0, T]; H^{k+3}(\Omega))} + \|(Lu)^{(j)}\|_{L^2([0, T]; H^{k+2}(\Omega))}), \\ \|u_h - u\|_{L^\infty([0, T]; L^2(\Omega))} &\leq Ch^{k+2} \sum_{j=0}^1 (\|u^{(j)}\|_{L^\infty([0, T]; H^{k+3}(\Omega))} + \|(Lu)^{(j)}\|_{L^\infty([0, T]; H^{k+2}(\Omega))}), \end{aligned}$$

418 where  $C$  is independent of  $t, h, u$ , and  $f$ .

419 *Proof.* As in the parabolic case we start by estimating  $\theta_h$ .

$$420 \quad (5.17) \quad \langle \theta_h^{(1)}, v_h \rangle_h + i\langle \nabla \theta_h, \nabla v_h \rangle_h + i\langle V\theta_h, v_h \rangle_h = -\langle \rho_h^{(1)}, v_h \rangle_h + \langle u^{(1)} - u_p^{(1)}, v_h \rangle_h, \quad \forall v_h \in V_0^h.$$

421 Taking  $v_h = \theta_h$  in (5.17) and taking real part,

$$422 \quad \begin{aligned} \frac{d}{dt} \|\theta_h\|_{l^2(\Omega)}^2 &= \frac{d}{dt} \langle \theta_h, \theta_h \rangle_h = 2\operatorname{Re} \left( -\langle \rho_h^{(1)}, \theta_h \rangle_h + \langle u^{(1)} - u_p^{(1)}, \theta_h \rangle_h \right) \\ &\leq 2 \left( \|\rho_h^{(1)}\|_{l^2(\Omega)} + \|u^{(1)} - u_p^{(1)}\|_{l^2(\Omega)} \right) \|\theta_h\|_{l^2(\Omega)}. \end{aligned}$$

423  
424

425 Since  $\frac{d}{dt} \|\theta_h\|_{l^2(\Omega)}^2 = 2\|\theta_h\|_{l^2(\Omega)} \frac{d}{dt} \|\theta_h\|_{l^2(\Omega)}$ , it implies

$$426 \quad \frac{d}{dt} \|\theta_h\|_{l^2(\Omega)} \leq \|\rho_h^{(1)}\|_{l^2(\Omega)} + \|u^{(1)} - u_p^{(1)}\|_{l^2(\Omega)}.$$

428 Upon integrating this inequality with respect to  $t$  from 0 to  $s$  we have

$$429 \quad \|\theta_h(s)\|_{l^2(\Omega)} \leq \|\theta_h(0)\|_{l^2(\Omega)} + \int_0^s (\|\rho_h^{(1)}\|_{l^2(\Omega)} + \|u^{(1)} - u_p^{(1)}\|_{l^2(\Omega)}) dt.$$

431 Now, using Theorem 3.1, (4.3), and (2.8) we have

$$432 \quad \begin{aligned} \|\theta_h(0)\|_{l^2} &= \|(u_0)_I - (R_h u)(0)\|_{l^2} \\ 433 \quad &= \|(u_0)_I - (u_0)_p + (u_0)_p - (R_h u)(0)\|_{l^2} \\ 434 \quad &\leq \|(u_0)_I - (u_0)_p\|_{l^2} + \|(u_0)_p - (R_h u)(0)\|_{l^2} \\ 435 \quad &= \|u_0 - (u_0)_p\|_{l^2} + \|(u_0)_p - R_h u_0\|_{l^2} \\ 436 \quad &= \mathcal{O}(h^{k+2})(\|u_0\|_{k+3} + \|Lu_0\|_{k+2}). \end{aligned}$$

438 With this result in concert with (4.2), (4.3), and Theorem 3.1 we note

$$439 \quad \|\theta_h(s)\|_{l^2(\Omega)} \leq \mathcal{O}(h^{k+2}) \left( \|u_0\|_{k+3} + \|Lu_0\|_{k+2} + \int_0^s \sum_{j=0}^1 (\|u^{(j)}\|_{k+3} + \|(Lu)^{(j)}\|_{k+2}) dt \right).$$

440 Together with (4.2), (4.3), and Theorem 3.1, proof is concluded.  $\square$

441 **5.4. Neumann boundary conditions and  $\ell^\infty$ -norm estimate.** For homo-  
 442 geneous Neumann type boundary conditions, due to Lemma 3.3, in general we can  
 443 only prove  $(k + \frac{3}{2})$ -th order accuracy for the hyperbolic equation, parabolic equation,  
 444 and linear Schrödinger equation. As explained in Remark 3.7, the half order loss  
 445 happens for homogeneous Neumann boundary condition only when the second order  
 446 operator coefficient  $\mathbf{a}$  is not diagonal, e.g., when the PDE contains second order mixed  
 447 derivatives. If  $\mathbf{a}$  is diagonal, then all results of  $(k + 2)$ -th order in  $\ell^2$  norm in this Sec-  
 448 tion can be easily extended to the homogeneous Neumann boundary conditions. See  
 449 Section 2.8 in [22] for a detailed discussion of nonhomogeneous Neumann boundary  
 450 conditions.

451 For Lagrangian  $Q^k$  finite element method without any quadrature solving the  
 452 elliptic equation with Dirichlet boundary conditions, the best superconvergence order  
 453 in max norm of function values at Gauss-Lobatto that one can prove is  $\mathcal{O}(|\log h|h^{k+2})$   
 454 in two dimensions, see [24] and references therein. Thus we do not expect better results  
 455 can be proven in the  $Q^k$  spectral element method in  $\ell^\infty$  norm over all nodes of degree  
 456 of freedoms.

457 **6. The implementation for nonhomogeneous Dirichlet boundary con-**  
 458 **ditions.** Consider the hyperbolic problem on  $\Omega = (0, 1)^2$  with compatible nonhomo-  
 459 geneous Dirichlet boundary condition and initial value

$$460 \quad (6.1) \quad \begin{aligned} u_{tt} &= -Lu + f(\mathbf{x}, t) && \text{in } \Omega \times (0, T], \\ u(\mathbf{x}, t) &= g && \text{on } \partial\Omega \times [0, T], \\ u(\mathbf{x}, 0) &= u_0(\mathbf{x}), \quad u_t(\mathbf{x}, 0) = u_1(\mathbf{x}) && \text{on } \Omega \times \{t = 0\}. \end{aligned}$$

461 As in [12, 24], by abusing notation, we define

$$462 \quad g(x, y, t) = \begin{cases} 0, & \text{if } (x, y) \in (0, 1) \times (0, 1), \\ g(x, y, t), & \text{if } (x, y) \in \partial\Omega, \end{cases}$$



463 and define  $g_I \in V^h$  as the  $Q^k$  Lagrange interpolation at  $(k+1) \times (k+1)$  Gauss-  
 464 Lobatto points for each cell on  $\Omega$  of  $g(x, y, t)$ . Namely,  $g_I \in V^h$  is the piecewise  $Q^k$   
 465 interpolant of  $g$  along  $\partial\Omega$  at the boundary grid points and  $g_I = 0$  at the interior grid  
 466 points. Then the semi-discrete scheme for problem (6.1) is as follows: for  $t \in [0, T]$ ,  
 467 find  $\tilde{u}_h \in V_0^h$  such that

$$468 \quad (6.2) \quad \begin{aligned} & \langle \tilde{u}_h^{(2)}, v_h \rangle_h + A_h(\tilde{u}_h, v_h) = \langle f, v_h \rangle_h - A_h(g_I, v_h), \quad \forall v_h \in V_0^h, \\ & \tilde{u}_h(0) = R_h u_0, \quad \tilde{u}_h^{(1)}(0) = (u_1)_I. \end{aligned}$$

469 Then

$$470 \quad (6.3) \quad u_h := \tilde{u}_h + g_I,$$

471 is the desired numerical solution. Notice that  $u_h$  and  $\tilde{u}_h$  are the same at all interior  
 472 grid points.

473 For the initial value of numerical solution, instead of using discrete elliptic pro-  
 474 jection, we can also use  $\tilde{u}_h(0) = u(x, y, 0)_I$  in (6.2) where  $u(x, y, 0)_I$  is the piecewise  
 475 Lagrangian  $Q^k$  interpolation of  $u(x, y, 0)$ . In all numerical tests in Section 7,  $(k+2)$ -th  
 476 order accuracy is still observed for the initial condition  $\tilde{u}_h(0) = u(x, y, 0)_I$ .

477 The treatment for nonhomogeneous Dirichlet boundary condition above can be  
 478 extended naturally to the parabolic equation and linear Schrödinger equation,

479 **REMARK 6.1.** *For the  $(k+2)$ -th order accuracy of the scheme (6.2), it can be*  
 480 *shown analogously as in [24], and in Section 4 and Section 5 by defining discrete*  
 481 *elliptic projection as*

$$482 \quad (6.4) \quad R_h u := \tilde{R}_h u + g_I,$$

483 where  $\tilde{R}_h u \in V_0^h$  satisfying

$$484 \quad A_h(\tilde{R}_h u, v_h) = \langle -Lu, v_h \rangle_h - A_h(g_I, v_h), \quad \forall v_h \in V_0^h, \quad 0 \leq t \leq T.$$

485 **7. Numerical examples.** In this section we present numerical examples for the  
 486 wave equation, a parabolic equation and the Schrödinger equation.

### 487 7.1. Numerical examples for the wave equation.

488 **7.1.1. Timestepping.** The so called modified equation technique, [10, 35, 16,  
 489 19], is an attractive option for timestepping the scalar wave equation. After semidis-  
 490 cretization the method (2.6) can be written as

$$491 \quad \frac{d^2 \mathbf{u}_h}{dt^2} = Q \mathbf{u}_h,$$

492 where  $\mathbf{u}_h$  is a vector containing all the degrees of freedom and  $Q$  is a matrix. To  
 493 evolve in time we expand the approximate solution around  $t + \Delta t$  and  $t - \Delta t$

$$494 \quad \mathbf{u}_h(t + \Delta t) + \mathbf{u}_h(t - \Delta t) = 2\mathbf{u}_h(t) + \Delta t^2 \frac{d^2 \mathbf{u}_h(t)}{dt^2} + \frac{\Delta t^4}{12} \frac{d^4 \mathbf{u}_h(t)}{dt^4} + \frac{\Delta t^6}{360} \frac{d^6 \mathbf{u}_h(t)}{dt^6} + \mathcal{O}(\Delta t^8).$$

495 Replacing the even time derivatives with applications of the matrix  $Q$  we obtain, for  
 496 example, a 6th order accurate explicit temporal approximation

$$497 \quad \mathbf{u}_h(t + \Delta t) + \mathbf{u}_h(t - \Delta t) = 2\mathbf{u}_h(t) + \Delta t^2 Q \mathbf{u}_h(t) + \frac{\Delta t^4}{12} Q^2 \mathbf{u}_h(t) + \frac{\Delta t^6}{360} Q^3 \mathbf{u}_h(t).$$

498 Note that the matrix  $Q$  does not need to be explicitly known, and an implicit  
 499 definition through a “matrix-vector multiplication” subroutine will suffice. In that  
 500 case the three last terms on the right hand side of the above equation would be  
 501 computed by repeated application of  $Q$ . For example to compute  $\mathbf{u}_h(t+\Delta t)$  one would  
 502 assign  $\mathbf{v}_h = 2\mathbf{u}_h(t) - \mathbf{u}_h(t - \Delta t)$ ,  $\mathbf{u}_h(t - \Delta t) = \mathbf{u}_h(t)$ , followed by three applications  
 503 of  $Q$  and updates of  $\mathbf{v}_h$ : (1)  $\mathbf{w}_h = Q\mathbf{u}_h(t)$ ,  $\mathbf{v}_h \leftarrow \mathbf{v}_h + \Delta t^2\mathbf{w}_h$ ,  $\mathbf{u}_h(t) = \mathbf{w}_h$ , (2)  
 504  $\mathbf{w}_h = Q\mathbf{u}_h(t)$ ,  $\mathbf{v}_h \leftarrow \mathbf{v}_h + \Delta t^4/12\mathbf{w}_h$ ,  $\mathbf{u}_h(t) = \mathbf{w}_h$ , (3)  $\mathbf{w}_h = Q\mathbf{u}_h(t)$ ,  $\mathbf{v}_h \leftarrow \mathbf{v}_h +$   
 505  $\Delta t^6/360\mathbf{w}_h$ . The time update is then finalized by the assignment  $\mathbf{u}_h(t) = \mathbf{v}_h$ , which  
 506 can conveniently be implemented as a for loop.

507 **7.1.2. Standing mode with Dirichlet conditions.** In this experiment we  
 508 solve the the wave equation  $u_{tt} = u_{xx} + u_{yy}$  with homogenous Dirichlet boundary  
 509 conditions in the square domain  $(x, y) \in [-\pi, \pi]^2$ . We take the initial data to be

$$510 \quad u(x, y, 0) = \sin(x) \sin(y), \quad u_t(x, y, 0) = 0,$$

511 which results in the exact standing mode solution

$$512 \quad u(x, y, 0) = \sin(x) \sin(y) \cos(\sqrt{2}t).$$

513 We consider the two cases  $k = 2$  and  $k = 4$  and discretize on three different  
 514 sequences of grids. The first sequence contains only plain Cartesian of increasing re-  
 515 finement. The second sequence consists of the same grids as in the Cartesian sequence  
 516 but with all the interior nodes perturbed by a two dimensional uniform random vari-  
 517 able with each component drawn from  $[-h/4, h/4]$ . The nodes of the third sequence  
 518 are

$$519 \quad (x, y) = (\xi + 0.1 \sin(\xi) \sin(\eta), \eta + 0.1 \sin(\eta) \sin(\xi)), \quad (\xi, \eta) = [-\pi, \pi]^2,$$

520 and this is refined in the same ways as the Cartesian sequence. Typical examples of  
 521 the grids are displayed in Figure 1. Even though the equation contains no coefficients,  
 522 variable coefficients are still involved for the second and the third sequences of grids.  
 523 The variable coefficients are induced by the geometric transformations of the elements  
 524 in the mesh to a reference rectangle element. However, on a randomly perturbed grid,  
 525 the variable coefficients are not smooth across cell interfaces. The variable coefficients  
 526 are smooth in a smoothly perturbed grid.

527 We evolve the numerical solution until time 5 by the time stepping discussed in  
 528 Section 7.1.1 of order of accuracy 4 when  $k = 2$  and 6 when  $k = 4$ . To get clean  
 529 measurements of the error we report the time integrated errors

$$530 \quad \left( \int_0^5 \|u(\cdot, t) - u_h(\cdot, t)\|_{l^2}^2 dt \right)^{\frac{1}{2}}, \quad \int_0^5 \|u(\cdot, t) - u_h(\cdot, t)\|_{l^\infty} dt,$$

531 for the spatial  $l^2$  and  $l^\infty$  errors respectively.

532 The results are displayed in Figure 2. Note that here and in the rest of this section  
 533 the solid lines in the figures are the computed errors, using many different grid sizes,  
 534 and the symbols are indicating the slopes or rates of convergence of the curves. The  
 535 Cartesian grids and smoothly perturbed grids satisfy the assumptions of the theory  
 536 developed in this paper while the second sequence of randomly perturbed grids does  
 537 not. The results confirm the theoretical predictions for smooth variable coefficients as  
 538 the rate of convergence is  $k + 2$  for the  $l^2$ -norm in the cases of the Cartesian meshes  
 539 and the smoothly perturbed meshes. We also observe the rate  $k + 2$  in the  $l^\infty$ -norm

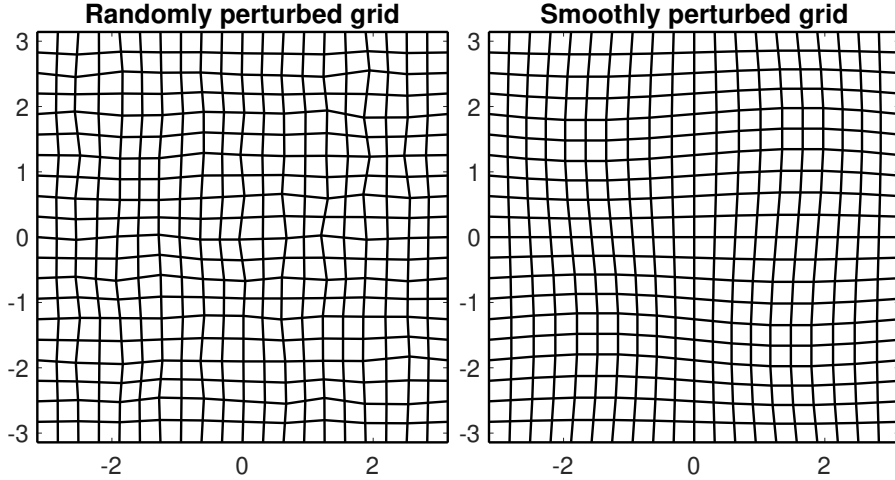


FIG. 1. Two typical grids used in the numerical examples in Section 7.1.2 and 7.1.4.

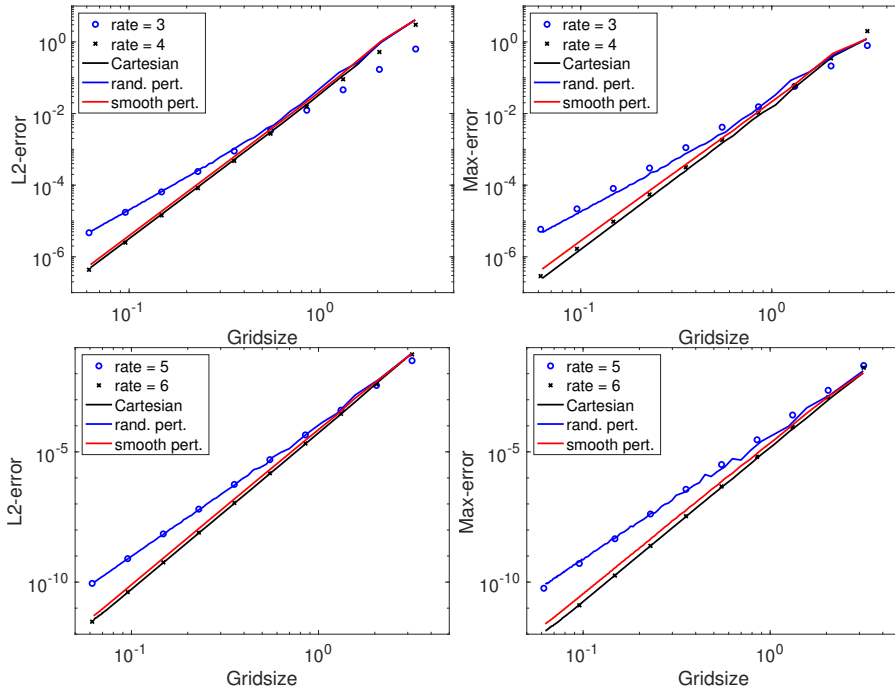


FIG. 2. Dirichlet problem in a square. Errors measured in the  $l^2$  and the  $l^\infty$  norms for the three different sequences of grids. The top row is for  $k = 2$  and the bottom row is for  $k = 4$ .

540 for these cases. For the non-smooth variable coefficients resulting from the randomly  
 541 perturbed grid, which is not covered by our theory, we see a rate of convergence of  
 542  $k + 1$  in the  $l^2$ -norm.

543 **7.1.3. Standing mode in a sector of an annulus with Dirichlet condi-**  
 544 **tions.** In this experiment we solve the wave equation  $u_{tt} = u_{xx} + u_{yy}$  with homoge-  
 545 nous Dirichlet boundary conditions. The computational domain is the first quadrant

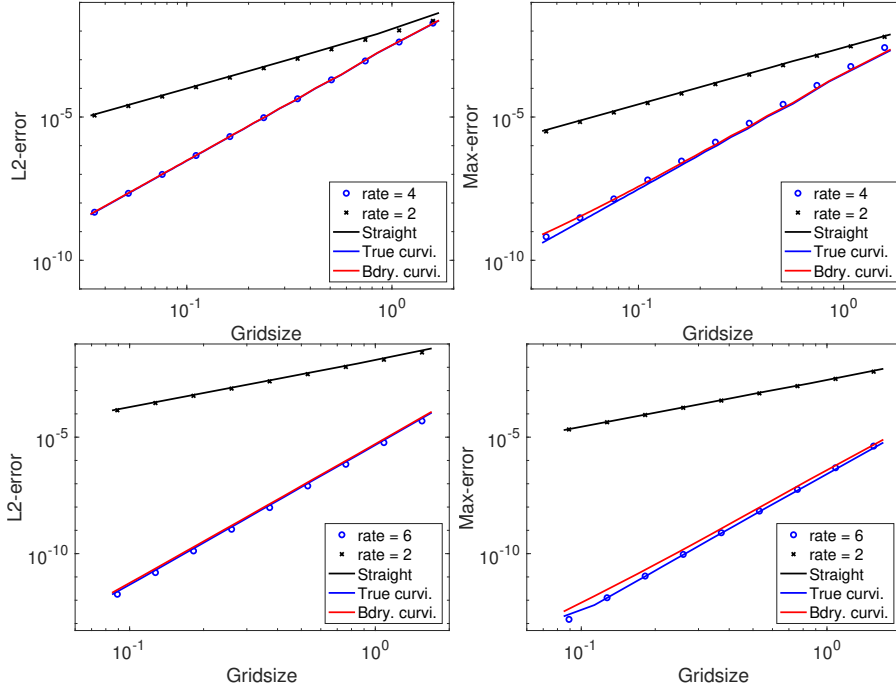


FIG. 3. *Dirichlet problem in an annular sector. Errors measured in the  $l^2$  and the  $l^\infty$  norms for the three different sequences of grids. The top row is for  $k = 2$  and the bottom row is for  $k = 4$ . These results are for the annular problem with homogenous Dirichlet boundary conditions.*

546 of the annular region between two circles with radii  $r_i = 7.58834243450380438$  and  
 547  $r_o = 14.37253667161758967$ , i.e. the domain is described by  $(x, y) = (r \cos \theta, r \sin \theta)$   
 548 where

$$549 \quad r_i \leq r \leq r_o, \quad 0 \leq \theta \leq \pi/2.$$

550 On this domain the standing mode

$$551 \quad u(r, \theta, t) = J_4(r) \sin(4\theta) \cos(t),$$

552 is an exact solution and we use this solution to specify the initial conditions and to  
 553 compute errors.

554 We consider the two cases  $k = 2$  and  $k = 4$  and discretize on three different  
 555 sequences of grids. The first sequence uses a straight sided approximation of the  
 556 annulus and all internal elements are quadrilaterals with straight sides. The second  
 557 sequence uses curvilinear elements throughout the domain and all internal element  
 558 boundaries conform with the polar coordinate transformation. After the smooth  
 559 mapping to the unit square, smooth variable coefficients emerge due to the geometric  
 560 terms. The metric terms are approximated with numerical differentiation using the  
 561 values at the quadrature points. The third sequence is the same as the second sequence  
 562 but all the internal element edges are straight. The meshes in the last sequence are  
 563 likely close to those that would be provided by most grid generators.

564 We evolve the numerical solution until time 1 by the time stepping discussed in  
 565 Section 7.1.1 of order of accuracy 4 when  $k = 2$  and 6 when  $k = 4$ . Again, to get

566 clean measurements of the error we report the time integrated errors

$$567 \quad \left( \int_0^1 \|u(\cdot, t) - u_h(\cdot, t)\|_{l^2}^2 dt \right)^{\frac{1}{2}}, \quad \int_0^1 \|u(\cdot, t) - u_h(\cdot, t)\|_{l^\infty} dt,$$

568 for the spatial  $l^2$  and  $l^\infty$  errors respectively.

569 The results are displayed in Figure 3. Here, as expected, we only observe second  
 570 order accuracy independent of  $k$  for the non-geometry-conforming meshes. We observe  
 571 a convergence at the rate of  $k + 2$  in both the  $l^2$ -norm and  $l^\infty$ -norm for the geometry-  
 572 conforming meshes. The true curvilinear grids are covered by our theory since the  
 573 variable coefficients due to the geometric transformation are smooth. For the third  
 574 sequence of grids, since internal edges are straightsided, the variable coefficients from  
 575 the geometric transformation are not smooth across edges thus this configuration is  
 576 not covered by our theory. Nonetheless, its convergence rate is still  $k + 2$ .

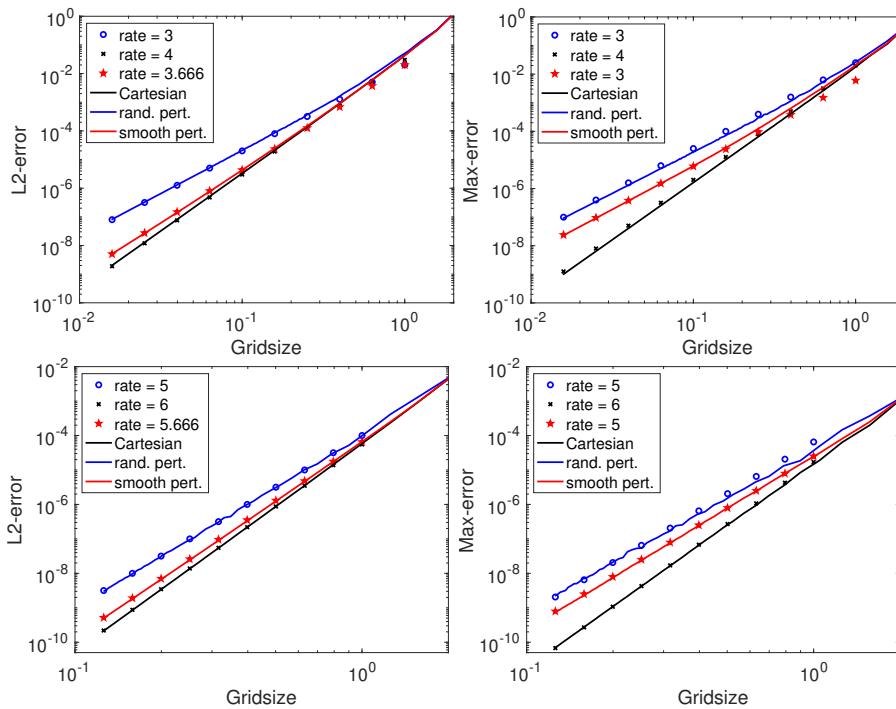


FIG. 4. Neumann square problem. Errors measured in the  $l^2$  and the  $l^\infty$  norms for the three different sequences of grids. The top row is for  $k = 2$  and the bottom row is for  $k = 4$ .

577 **7.1.4. Standing mode with Neumann conditions.** In this experiment we  
 578 approximate the solution to the wave equation  $u_{tt} = u_{xx} + u_{yy}$  in the square domain  
 579  $(x, y) \in [-\pi, \pi]^2$ . Then with homogenous Neumann boundary conditions and initial  
 580 data

$$581 \quad u(x, y, 0) = \cos(x) \cos(y), \quad u_t(x, y, 0) = 0,$$

582 the exact standing mode solution is

$$583 \quad u(x, y, 0) = \cos(x) \cos(y) \cos(\sqrt{2}t).$$

584 We consider the two cases  $k = 2$  and  $k = 4$  and discretize on the same three  
 585 sequences of grids as those used in §7.1.2. We evolve the numerical solution until time  
 586 5 as above and we report the time integrated errors as above.

587 The results are displayed in Figure 4. For the Cartesian mesh we observe a rate of  
 588 convergence  $k + 2$  in the  $\ell^2$ -norm, confirming our theory. For the smoothly perturbed  
 589 grids, which corresponds to smooth variable coefficients resulting in mixed second  
 590 order derivatives on the reference rectangular mesh, the rate in the  $l^2$ -norm appears  
 591 to be  $k + 5/3$ . As explained in Section 5.4, only  $(k + \frac{3}{2})$ -th order can be proven when  
 592 both mixed second order derivatives and Neumann boundary conditions are involved.  
 593 As in the Dirichlet case, the randomly perturbed grid yields rates of convergence  $k + 1$   
 594 in both norms.

595 **7.1.5. Standing mode in a sector of an annulus with Neumann con-**  
 596 **ditions.** In this experiment we solve the the wave equation  $u_{tt} = u_{xx} + u_{yy}$  with  
 597 homogenous Neumann boundary conditions. The computational domain is again  
 598 the first quadrant of the annular region between two circles, now with radii  $r_i =$   
 599  $5.31755312608399$  and  $r_o = 9.28239628524161$ , to satisfy the boundary conditions.  
 600 On this domain the standing mode

$$601 \quad u(r, \theta, t) = J_4(r) \cos(4\theta) \cos(t),$$

602 is an exact solution and we use this solution to specify the initial conditions and to  
 603 compute errors.

604 As in the previous examples we consider the two cases  $k = 2$  and  $k = 4$  and  
 605 discretize on the same three different sequences of grids as was used in the Dirichlet  
 606 example above. We evolve the numerical solution until time 1 in the same way as  
 607 above and we report the time integrated errors.

608 The results are displayed in Figure 5. Here, the only grid satisfying our assump-  
 609 tions is the true curvilinear grid. For this case, the problem is equivalent to solving a  
 610 variable coefficient problem  $u_{tt} = u_{rr} + \frac{1}{r^2}u_{\theta\theta} + \frac{1}{r}u_r$  on rectangular meshes for polar  
 611 coordinates  $(r, \theta) \in [r_i, r_o] \times [0, \frac{\pi}{2}]$ . Since there are no mixed second order derivatives,  
 612 by our theory as explained in Section 5.4,  $(k + 2)$ -th order in the  $\ell^2$ -norm can still  
 613 be proven. We can see that the rate for the true curvilinear grid is indeed  $k + 2$  in  
 614  $\ell^2$ -norm, confirming our theory for Neumann boundary conditions.

615 **7.2. Numerical tests for the parabolic equation.** For problem (2.1) on the  
 616 domain  $\Omega = (0, \pi)^2$ , we set  $\mathbf{a} = \begin{pmatrix} a_{11} & a_{12} \\ a_{21} & a_{22} \end{pmatrix}$  with

$$a_{11} = \left( \frac{3}{4} + \frac{1}{4} \sin(t) \right) (1 + y + y^2 + x \cos y),$$

$$617 \quad a_{12} = a_{21} = \left( \frac{3}{4} + \frac{1}{4} \sin(t) \right) \left( 1 + \frac{1}{2} (\sin(\pi x) + x^3) (\sin(\pi y) + y^3) + \cos(x^4 + y^3) \right),$$

$$a_{22} = \left( \frac{3}{4} + \frac{1}{4} \sin(t) \right) (1 + x^2),$$

$$618 \quad \mathbf{b} = \begin{pmatrix} b_1 \\ b_2 \end{pmatrix} \text{ with}$$

$$619 \quad b_1 = \left( \frac{3}{4} + \frac{1}{4} \sin(t) \right) \left( \frac{1}{5} + x \right), b_2 = \left( \frac{3}{4} + \frac{1}{4} \sin(t) \right) \left( \frac{1}{5} - y \right),$$

620 and  $c = \left( \frac{3}{4} + \frac{1}{4} \sin(t) \right) (10 + x^4 y^3)$ . For time discretization in (2.5), we use the  
 621 third order backward differentiation formula (BDF) method. Let  $u(x, y, t) = \left( \frac{3}{4} +$

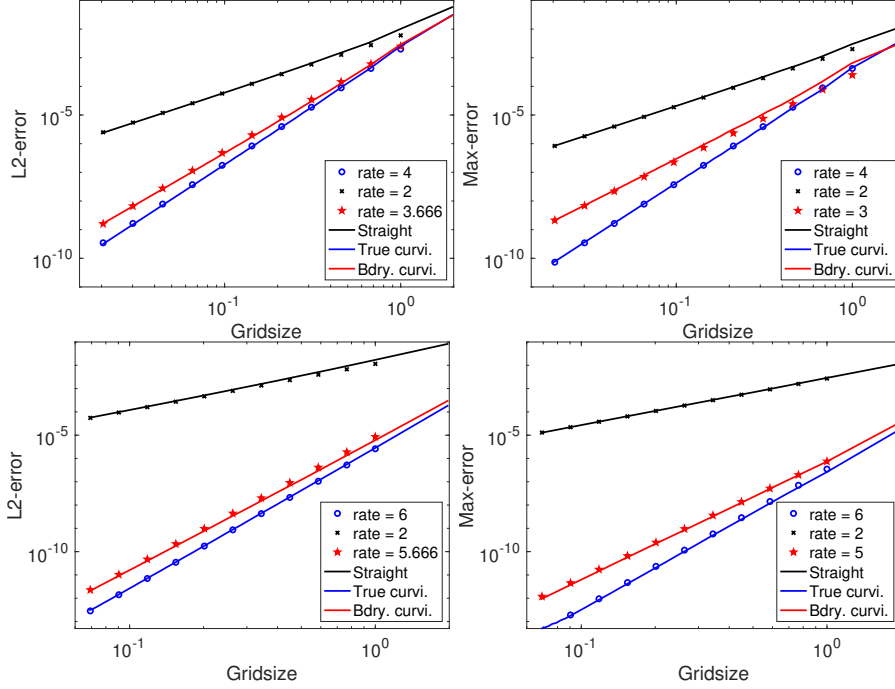


FIG. 5. Neumann annular sector problem. Errors measured in the  $l^2$  and the  $l^\infty$  norms for the three different sequences of grids. The top row is for  $k = 2$  and the bottom row is for  $k = 4$ . These results are for the annular problem with homogenous Neumann conditions.

622  $\frac{1}{4} \sin(t)(-\sin(y) \cos(y) \sin(x)^2)$  and we use a potential function  $f$  so that  $u$  is the  
 623 exact solution. The time step is set as  $\Delta t = \min(\frac{\Delta x}{10}, \frac{\Delta x}{10b_M}, \frac{f_M}{10})$ , where  $b_M =$   
 624  $\max_{\mathbf{x} \in \Omega, i=1,2} |b_i(0, \mathbf{x})|$  and  $f_M = \max_{\mathbf{x} \in \Omega} |f(0, \mathbf{x})|$ . The errors at time  $T = 0.1$  are  
 625 listed in Table 1, in which we observe order around  $k + 2$  for the  $\ell^2$ -norm.

TABLE 1  
 A two-dimensional parabolic equation with Dirichlet boundary conditions.

$Q^k$ polynomial	SEM Mesh	$l^2$ error	order	$l^\infty$ error	order
k = 2	$4 \times 4$	8.34E-3	-	4.57E-3	-
	$8 \times 8$	6.59E-4	3.66	3.16E-4	3.85
	$16 \times 16$	4.52E-5	3.86	2.36E-5	3.74
	$32 \times 32$	2.91E-6	3.96	1.53E-6	3.94
k = 3	$4 \times 4$	5.88E-4	-	1.71E-4	-
	$8 \times 8$	2.24E-5	4.71	7.56E-6	4.50
	$16 \times 16$	7.49E-7	4.90	2.52E-7	4.91
	$32 \times 32$	2.38E-8	4.97	8.06E-9	4.96
k = 4	$4 \times 4$	4.26E-5	-	1.16E-5	-
	$8 \times 8$	7.62E-7	5.81	2.34E-7	5.63
	$16 \times 16$	1.26E-8	5.92	4.12E-9	5.83
	$32 \times 32$	2.00E-10	5.98	6.68E-11	5.95

626 **7.3. Numerical tests for the linear Schrödinger equation.** For problem  
 627 (5.13) on the domain  $(0, 2)^2$ , a fourth-order explicit Adams-Bashforth as time dis-  
 628 cretization for (5.15). The solution and potential functions are as follows:  $u(x, y, t) =$   
 629  $e^{-it} e^{-\frac{x^2+y^2}{2}}$ ,  $V(x, y) = \frac{x^2+y^2}{2}$ , and  $f(x, y, t) = 0$ . The time step is set as  $\Delta t = \frac{\Delta x^2}{500}$ .  
 630 Errors at time  $T = 0.5$  are listed in Table 2, in which we observe order near  $k + 2$  for  
 631 the  $\ell^2$ -norm.

TABLE 2  
*A two-dimensional linear Schrödinger equation with Dirichlet boundary conditions.*

$Q^k$ polynomial	SEM Mesh	$l^2$ error	order	$l^\infty$ error	order
k = 2	$4 \times 4$	9.98E-4	-	6.36E-4	-
	$8 \times 8$	6.65E-5	3.91	4.01E-5	3.99
	$16 \times 16$	4.10E-6	4.02	2.77E-6	3.85
	$32 \times 32$	2.53E-7	4.02	1.79E-7	3.89
k = 3	$4 \times 4$	4.06E-5	-	2.12E-5	-
	$8 \times 8$	1.12E-6	5.18	5.56E-7	5.26
	$16 \times 16$	3.22E-8	5.12	1.75E-8	4.99
	$32 \times 32$	1.05E-9	4.94	5.33E-10	5.04
k = 4	$4 \times 4$	1.61E-6	-	5.86E-7	-
	$8 \times 8$	2.65E-8	5.92	9.93E-9	5.88
	$16 \times 16$	3.95E-10	6.07	1.66E-10	5.90
	$32 \times 32$	5.30E-12	6.22	2.66E-12	5.97

632 **8. Concluding remarks.** We have proven that the  $Q^k$  ( $k \geq 2$ ) spectral element  
 633 method, when regarded as a finite difference scheme, is a  $(k + 2)$ -th order accurate  
 634 scheme in the discrete 2-norm for linear hyperbolic, parabolic and Schrödinger equa-  
 635 tions with Dirichlet boundary conditions, under smoothness assumptions of the exact  
 636 solution and the differential operator coefficients. The same result holds for Neumann  
 637 boundary conditions when there are no mixed second order derivatives. This explains  
 638 the observed order of accuracy when the errors of the spectral element method are  
 639 only measured at nodes of degree of freedoms.

#### REFERENCES

- 640
- 641 [1] M. ALMQUIST, S. WANG, AND J. WERPERS, Order-preserving interpolation for  
 642 summation-by-parts operators at nonconforming grid interfaces, SIAM J. Sci. Com-  
 643 put., 41 (2019), pp. A1201–A1227.
- 644 [2] D. APPELÖ AND T. HAGSTROM, A new discontinuous Galerkin formulation for wave equations  
 645 in second order form, SIAM Journal On Numerical Analysis, 53 (2015), pp. 2705–2726.
- 646 [3] C. CHEN, Structure theory of superconvergence of finite elements (In Chinese), Hunan Science  
 647 and Technology Press, Changsha, 2001.
- 648 [4] K. CHENG, W. FENG, S. GOTTLIEB, AND C. WANG, A Fourier pseudospectral method for the  
 649 good Boussinesq equation with second-order temporal accuracy, Numerical Methods for  
 650 Partial Differential Equations, 31 (2015), pp. 202–224.
- 651 [5] K. CHENG, C. WANG, AND S. M. WISE, An energy stable BDF2 Fourier pseudo-spectral  
 652 numerical scheme for the square phase field crystal equation.
- 653 [6] C.-S. CHOU, C.-W. SHU, AND Y. XING, Optimal energy conserving local discontinuous Galerkin  
 654 methods for second-order wave equation in heterogeneous media, Journal of Computational  
 655 Physics, 272 (2014), pp. 88–107.
- 656 [7] E. T. CHUNG AND B. ENQUIST, Optimal discontinuous Galerkin methods for wave propagation,  
 657 SIAM Journal on Numerical Analysis, 44 (2006), pp. 2131–2158.



- 658 [8] E. T. CHUNG AND B. ENGQUIST, Optimal discontinuous Galerkin methods for the acoustic  
659 wave equation in higher dimensions, SIAM Journal on Numerical Analysis, 47 (2009),  
660 pp. 3820–3848.
- 661 [9] G. COHEN, Higher-order numerical methods for transient wave equations, Springer Science &  
662 Business Media, 2001.
- 663 [10] M. A. DABLAIN, The application of high-order differencing to the scalar wave equation, Geo-  
664 physics, 51 (1986), pp. 54–66.
- 665 [11] T. DUPONT,  $L^2$ -estimates for Galerkin methods for second order hyperbolic equations, SIAM  
666 journal on numerical analysis, 10 (1973), pp. 880–889.
- 667 [12] M. S. GOCKENBACH, Understanding and implementing the finite element method, vol. 97, Siam,  
668 2006.
- 669 [13] S. GOTTLIEB AND C. WANG, Stability and convergence analysis of fully discrete Fourier  
670 collocation spectral method for 3-D viscous Burgers equation, Journal of Scientific Com-  
671 puting, 53 (2012), pp. 102–128.
- 672 [14] P. GRISVARD, Elliptic problems in nonsmooth domains, vol. 69, SIAM, 2011.
- 673 [15] M. J. GROTE, A. SCHNEEBELI, AND D. SCHÖTZAU, Discontinuous Galerkin finite element  
674 method for the wave equation, SIAM Journal on Numerical Analysis, 44 (2006), pp. 2408–  
675 2431.
- 676 [16] W. D. HENSHAW, A high-order accurate parallel solver for Maxwell’s equations on overlapping  
677 grids, SIAM Journal on Scientific Computing, 28 (2006), pp. 1730–1765.
- 678 [17] J. HESTHAVEN AND T. WARBURTON, Nodal high-order methods on unstructured grids: I.  
679 time-domain solution of Maxwell’s equations, J. Comput. Phys., 181 (2002), pp. 186–221.
- 680 [18] J. HESTHAVEN AND T. WARBURTON, Nodal Discontinuous Galerkin Methods, no. 54 in Texts  
681 in Applied Mathematics, Springer-Verlag, New York, 2008.
- 682 [19] P. JOLY AND J. RODRÍGUEZ, Optimized higher order time discretization of second order  
683 hyperbolic problems: Construction and numerical study, Journal of Computational and  
684 Applied Mathematics, 234 (2010), pp. 1953–1961.
- 685 [20] D. KOMATITSCH AND J. TROMP, Introduction to the spectral element method for  
686 three-dimensional seismic wave propagation, Geophysical journal international, 139 (1999),  
687 pp. 806–822.
- 688 [21] D. KOMATITSCH, J.-P. VILOTTE, R. VAI, J. M. CASTILLO-COVARRUBIAS, AND F. J. SÁNCHEZ-  
689 SESMA, The spectral element method for elastic wave equations: application to 2-D and 3-D  
690 seismic problems, International Journal for numerical methods in engineering, 45 (1999),  
691 pp. 1139–1164.
- 692 [22] H. LI, Accuracy and Monotonicity of Spectral Element Method on Structured Meshes, PhD  
693 thesis, Purdue University, 2021.
- 694 [23] H. LI AND X. ZHANG, Superconvergence of  $C^0 - Q^k$  finite element method for elliptic equations  
695 with approximated coefficients, Journal of Scientific Computing, 82 (2020), pp. 1–28.
- 696 [24] H. LI AND X. ZHANG, Superconvergence of high order finite difference schemes based on  
697 variational formulation for elliptic equations, Journal of Scientific Computing, 82 (2020),  
698 pp. 1–39.
- 699 [25] Q. LIN AND N. YAN, Construction and Analysis for Efficient Finite Element Method (In  
700 Chinese), Hebei University Press, 1996.
- 701 [26] Y. MADAY AND E. M. RØNQUIST, Optimal error analysis of spectral methods with emphasis  
702 on non-constant coefficients and deformed geometries, Computer Methods in Applied Me-  
703 chanics and Engineering, 80 (1990), pp. 91–115.
- 704 [27] K. MATTSSON, Summation by parts operators for finite difference approximations of  
705 second-derivatives with variable coefficients, Journal of Scientific Computing, 51 (2012),  
706 pp. 650–682.
- 707 [28] K. MATTSSON, F. HAM, AND G. IACCARINO, Stable and accurate wave-propagation in  
708 discontinuous media, J. Comput. Phys., 227 (2008), pp. 8753–8767.
- 709 [29] K. MATTSSON AND J. NORDSTRÖM, Summation by parts operators for finite difference  
710 approximations of second derivatives, J. Comput. Phys., 199 (2004), pp. 503–540.
- 711 [30] X. MENG, C.-W. SHU, AND B. WU, Optimal error estimates for discontinuous Galerkin methods  
712 based on upwind-biased fluxes for linear hyperbolic equations, Mathematics of Computa-  
713 tion, 85 (2016), pp. 1225–1261.
- 714 [31] P. MONK AND G. RICHTER, A discontinuous Galerkin method for linear symmetric hyperbolic  
715 systems in inhomogeneous media, Journal of Scientific Computing, 22-23 (2005), pp. 443–  
716 477.
- 717 [32] B. RIVIERE AND M. WHEELER, Discontinuous finite element methods for acoustic and elastic  
718 wave problems. part i: semidiscrete error estimates, Contemporary Mathematics, 329  
719 (2003), pp. 271–282.

- 720 [33] P. H. SAMMON, Convergence estimates for semidiscrete parabolic equation approximations,  
721 SIAM Journal on Numerical Analysis, 19 (1982), pp. 68–92.
- 722 [34] G. SAVARÉ, Regularity results for elliptic equations in Lipschitz domains, Journal of Functional  
723 Analysis, 152 (1998), pp. 176–201.
- 724 [35] G. R. SHUBIN AND J. B. BELL, A modified equation approach to constructing fourth order  
725 methods for acoustic wave propagation, SIAM J. Sci. Stat. Comput., 8 (1987), pp. 135–  
726 151, <https://doi.org/http://dx.doi.org/10.1137/0908026>.
- 727 [36] K. VIRTA AND K. MATTSSON, Acoustic wave propagation in complicated geometries and  
728 heterogeneous media, Journal of Scientific Computing, 61 (2014), pp. 90–118.
- 729 [37] L. WAHLBIN, Superconvergence in Galerkin finite element methods, Springer, 2006.
- 730 [38] S. WANG, An improved high order finite difference method for non-conforming grid interfaces  
731 for the wave equation, J. Sci. Comput., 77 (2018), pp. 775–792.
- 732 [39] S. WANG, K. VIRTA, AND G. KREISS, High order finite difference methods for the wave equation  
733 with non-conforming grid interfaces, Journal of Scientific Computing, 68 (2016), pp. 1002–  
734 1028.
- 735 [40] T. WARBURTON, A low-storage curvilinear discontinuous Galerkin method for wave problems,  
736 SIAM Journal on Scientific Computing, 35 (2013), pp. A1987–A2012.
- 737 [41] M. F. WHEELER, A priori  $L_2$  error estimates for Galerkin approximations to parabolic partial  
738 differential equations, SIAM Journal on Numerical Analysis, 10 (1973), pp. 723–759.